[23]M. Pollak and T. H. Geballe, Phys. Rev. <u>122</u>, 1742 (1961).

[24]*Handbook of Mathematical Functions*, edited by M. Abramowitz and I. A. Stegun (National Bureau of Standards, Washington, D. C., 1964).

[25]S. Tanaka and H. Y. Fan, Phys. Rev. <u>132</u>, 1516 (1963); S. Tabaka, M. Kobayashi, E. Hanamura, and K. Uchinokura, Phys. Rev. <u>134</u>, A256 (1964).

[26]L. Takás, *Stochastic Process* (Methuen, London, 1960); and Ref. 14.

[27]We are indebted to Dr. S. C. Maitra for a discussion of this subtle point as well as others in this Appendix.

[28]The W function, however, has the Poisson form for a fixed configuration; hence the RWRM is Markovian (cf. Refs. 26 and 19).

[29]D. G. Thomas, J. J. Hopfield, and W. M. Augustyniak, Phys. Rev. <u>140</u>, A202 (1965), Eqs. (17) and (18).

Stochastic Transport in a Disordered Solid. II. Impurity Conduction

H. Scher
Xerox Rochester Research Center, Xerox Square, Rochester, New York 14644

M. Lax
*City College of City University of New York, New York, New York 10031
and Bell Laboratories, Murray Hill, New Jersey 07974*
(Received 21 June 1972; revised manuscript received 30 November 1972)

In a previous paper, the authors have developed a general theory of stochastic transport in disordered systems. In the present paper, the theory is applied, in detail, to a prototype of transport in a disordered system – impurity conduction in semiconductors. The complete frequency dependence of the real and imaginary part of the conductivity is calculated. In particular, the calculation details the transition from an ω^s dependence to essentially dc behavior (at a finite frequency), where $s \sim 0.6-0.8$, depending on temperature and concentration. The theoretical results for frequency, temperature, and concentration dependence of the conductivity are shown to be in good agreement with the measurements of Pollak and Geballe (PG). In addition, the ac conductivity data of PG interpreted with the present theory yield experimental evidence for the existence of two-channel hopping in n-type Si.

I. INTRODUCTION

In the preceding paper[1] (hereafter referred to as I) a general theory of transport via localized states in a disordered system has been developed. The motion of the carriers in such a system has been modeled as a continuous-time random walk (CTRW) on a lattice.[2] The carrier executing such a CTRW makes a displacement $\vec{s}$ from each site in time t between steps with a distribution described by a function $\psi(\vec{s}, t)$. All the dynamics of the motion are incorporated into $\psi(\vec{s}, t)$. This simplification, inherent in the structure of the CTRW model, allows one to focus on the basic fluctuating quantity in the hopping motion—the transition rate between the sites. That is, the transition rate is treated as the random variable. For the transport in disordered systems of most interest, the transition rate is a very sensitive function of the intersite separation, so that the fluctuations in the spatial separation are quite mild compared to those, produced by them, in the transition rate. An extensive qualitative discussion of the nature of the present approach to hopping transport is included in the Introduction in I. The mathematical justification of the model is detailed in Appendix B in I.

For this CTRW model the conductivity $\sigma(\omega)$ has been determined exactly and is completely specified by the Fourier transform (FT) of the spatial moments of $\psi(\vec{s}, t)$,

$$\sigma_{rms}^2(\omega) \equiv \sum_{\vec{s}} s^2 \int_0^\infty e^{-i\omega t} \psi(\vec{s}, t) \, dt / \tilde{\psi}(i\omega) \tag{1}$$

and

$$\tilde{\psi}(i\omega) \equiv \sum_{\vec{s}} \int_0^\infty e^{-i\omega t} \psi(\vec{s}, t) \, dt . \tag{2}$$

Specifically,

$$D(\omega) = \tfrac{1}{6} \sigma_{rms}^2(\omega) \, i\omega \tilde{\psi}(i\omega) / [1 - \tilde{\psi}(i\omega)] , \tag{3}$$

where

$$\sigma(\omega) = (ne^2/\kappa T) D(\omega) , \tag{4}$$

n is the density of effective carriers (e.g., $n = N_A$, the acceptor concentration, in the case of impurity hopping in a low-compensated n-type semiconductor, to be discussed below), T is the absolute temperature, and $D(\omega)$ is the complex frequency-dependent diffusion constant.[1] In common units, e.g.,

$$D(\omega) \ (cm^2/sec) = (0.6723 \, T)[\sigma(\omega) \ (\Omega^{-1} cm^{-1})] \tag{5}$$

for $n = 8 \times 10^{14}$ cm^{-3}.

As one can readily observe from (3), knowledge of the FT of $\psi(\vec{s}, t)$ determines the linear response of the system to an electric field oscillating at angular frequency ω. Further, if one considers the limit $\omega \to 0$, one obtains

$$D(0) = \sigma_{rms}^2(0)/6\bar{t} , \qquad (6)$$

with

$$\bar{t} \equiv \int_0^\infty t\psi(t)\, dt , \qquad (7)$$

i.e., the dc resistivity of the system is proportional to the mean waiting time $\bar{t}$ for a typical hop (anywhere).

The existence of a finite dc limit for $\sigma(\omega)$ is a key feature of the present calculation and, as shown below, enables us to quantatively describe the "transition region" from an ω^s dependence to an essentially dc behavior (at finite ω) of the conductivity—a region that has not been previously described theoretically.

Now, in the present paper, we consider a detailed application of the theory to a prototype amorphous system—impurity hopping conduction[3,4] in semiconductors such as Si and Ge.[5-7] A great deal is known about this system—the impurity wave functions[8,9] and transition probabilities $W(\vec{r})$.[3,10] There is an extensive literature of experimental work[5-7,11,12] carried out on carefully characterized samples as well as some important theoretical studies.[3,4,13-16] Many key variables can be experimentally controlled to a large degree, e.g., the intersite distance.

In Sec. II, the basic features of impurity conduction are discussed in the context of an explicit calculation of $\psi(\vec{s}, t)$. First, a general procedure is developed for the calculation of $\psi(\vec{s}, t)$ from the transition rates $W(\vec{r})$ and the local site distribution. An analytic expression for $\psi(t)$ is then derived for a specific form of $W(\vec{r})$, and finally, an asymptotic evaluation of $\tilde{\psi}(i\omega)$ and hence $D(\omega)$ is made for two characteristic donor concentrations N_D. [In the present paper it will be assumed $\sigma_{rms}^2(\omega) \approx \sigma_{rms}^2(0)$ $\equiv \sigma_{rms}^2$. The quantitative aspects of the ω dependence of $\sigma_{rms}^2(\omega)$ will be treated in Ref. 19 of I.]

Some features of these results are (i) the complete frequency dependence of both the real and imaginary part of the conductivity is calculated. (ii) An analytic expression for the dc conductivity, derived with a simple form for $W(\vec{r})$, is similar to the Miller and Abrahams[3] (MA) result. This derivation does not make use of the resistive network model first introduced by MA and used in all subsequent theoretical calculations of $\sigma(0)$.[13,14] (iii) The pair approximation at higher frequency introduced by Pollak and Geballe[5] (PG) is not invoked in this model. All the multiple hops are included.

In Sec. III these theoretical results are compared

with the conductivity data of PG. The comparison is made separately for two characteristic concentrations N_D. At the lower concentration, the calculated frequency and temperature dependence of Re$\sigma(\omega)$ is in excellent agreement with the measurements of PG. In addition, strong evidence is advanced, in the context of the present theory, for two "channel" hopping in n-type phosphorous-doped Si. At the higher concentration and higher temperature $(T > 3.5\,^\circ$K$)$ the comparison with experiment is reproduced in Fig. 1. The solid line is the theoretical curve for the real part of a dimensionless diffusion constant $\bar{D}(\Omega) \equiv D(\omega)/\frac{1}{6}\sigma_{rms}^2 e^\gamma W_M$ plotted against a dimensionless frequency $\Omega \equiv \omega/W_M$, with W_M obtained from a simple expression for the transition rate $W(\vec{r}) = W_M e^{-2r/a}$, where a is the effective Bohr radius and $W_M \propto e^{-\Delta/\kappa T}$ and $\gamma = 0.5772$. The effective activation energy Δ is discussed in Sec. III and it suffices to say in Fig. 1 Δ is chosen to be equal to the experimental activation energy of the dc impurity conduction measured by PG. With this single value for Δ (therefore determining Ω for a given pair of values for ω and T), all of the data points, contained in Fig. 5 in PG, for $T > 3.5\,^\circ$K and for the range of values for $\omega/2\pi$ indicated in Fig. 1, are replotted as a function of Ω and shown to lie on a *universal* curve. The universal curve is a *simultaneous display of both the frequency and temperature dependence* of the ac diffusion measurements and it approximates well to the theoretical curve in Fig. 1. It should be stressed that there are no "fitted" parameters in the comparison in Fig. 1 (cf. Sec. III). A key feature of the results in Fig. 1 is the demonstration of a characteristic dimensionless "transition" frequency Ω_c. This frequency Ω_c depends only on N_D and a (cf. Sec. II) and earmarks the "transition
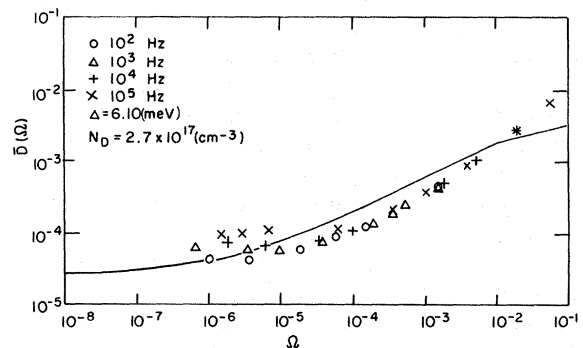
FIG. 1. Comparison of the theoretical (solid line) and experimental values of Re$\bar{D}(\Omega)$. The dimensionless diffusion constant $\bar{D}(\Omega) \equiv \sigma(\omega)/[(N_A e^2/\kappa T)(\frac{1}{6}\sigma_{rms}^2 e^\gamma W_M)]$, with $\gamma = 0.5772$; $\Omega \equiv \omega/W_M e^\gamma$, with W_M obtained from the transition rate $W(\vec{r}) = W_M \exp(-2r/a)$; a is the effective Bohr radius and $W_M \propto \exp(-\Delta/\kappa T)$. Data for Re$\sigma(\omega)$ taken from Pollak and Geballe, Ref. 5, Fig. 5. $N_A = 0.8 \times 10^{15}$ cm^{-3}, $N_D = 2.7 \times 10^{17}$ cm^{-3}, $\Delta = 6.1$ meV, $\sigma_{rms} = r_D \equiv (\frac{4}{3}\pi N_D)^{-1/3}$.

region" between a region where $\text{Re}\sigma(\omega) \propto \omega^s$ and a region where $\text{Re}\sigma(\omega) \propto \sigma(0)$. The details of Ω_c are discussed in Appendix B.

We conclude this section with a few general remarks about the nature of impurity hopping conduction. The underlying stochastic element in this transport process is intrinsically quantum mechanical. The wave function of the carrier is localized mainly about one impurity site with a small finite amplitude at another site. A transition between these sites can be induced by the electron-phonon interaction. The transition is therefore described by the nature of the charge distribution (e.g., the effective Bohr radius) around each impurity site, the electron-phonon coupling, and the perturbational addition to the charge distribution at the other site. The latter addition is largely determined by the energy difference between the states at the two sites and the overlap or resonance energy between them.[3] The sensitivity of the transition rate to the spatial separation of the sites comes in through the overlap energy. Thus, at each site in the course of time, the carrier can abruptly change its position to a number of others, each choice weighted by the quantum-mechanical transition matrix element described above. It is in this sense that the hopping transport *becomes a random walk on a random media*.

A random walk (RW) is a very general concept and simply depends on the existence of a recursive relation between the probability $p_n(i)$, of being in the state i after n "trials," and $P_{n-1}(j)$, where $j \neq i$. The connection between these two probabilities is simply the transition probability p_{ij} in a single "trial," i.e., $P_n(i) = \sum p_{ij} P_{n-1}(j)$, where the sum is over the specified set of states a_j excluding i.

For impurity conduction the hop corresponds to the "trial," the state i to the impurity site $\vec{s}_i$, a_j to the random network of sites $\vec{s}_j$ $(j \neq i)$, and p_{ij} to the probability the carrier on $\vec{s}_i$ hops to $\vec{s}_j$ $(p_{ij}$ can have an explicit dependence on $\vec{s}_i$, $\vec{s}_j$). In general, as discussed above, for impurity hopping transport p_{ij} is a sensitive function of $\vec{s}_i - \vec{s}_j$, so that the RW on the random distribution of sites can be closely approximated in a very elegant way by a percolation problem (for the dc case).[14] The basic idea behind this approach is to consider any two sites as "linked" (or joined with an open bond) if p_{ij} is greater than a specified value p_c. If $p_{ij} < p_c$ the sites $\vec{s}_i$, $\vec{s}_j$ are considered "unlinked." The "medium" determines the transport and the problem is reduced to finding p_c. The value p_c is then used to determine the conductivity σ_0 of the "critical" dc conducting path and σ_0, in turn, is equated with the dc impurity conductivity.

The approach in the present theory is to consider directly the RW problem with, however, two main modifications. The introduction of $\psi(\vec{s}, \tau)$, dis-

cussed above, accomplishes both of these changes: (i) The RW is generalized by replacing the discrete variable n (the number of trials or hops) by the continuous variable t (the time of observation of the carrier motion). Instead of $P_n(\vec{s}_i)$, one is concerned with $P(\vec{s}_i, t)$, the probability of finding the carrier at $\vec{s}_i$ at time t (cf. Sec. I of I). [The connection in this context to the quantum-mechanical nature of the hopping transport is shown in the formal definition of $P(\vec{s}_i, t)$ in Eq. (8) of I.] The underlying structure of the RW is still analyzed in terms of n (cf. Secs. I and III of I); however, each hop a distance $\vec{s}$ is allowed to occur at a random time τ with the distribution of $\psi(\vec{s}, \tau)$. The *explicit* consideration of t, i.e., the *dynamics* of impurity hopping, is the important factor in being able to treat the ac and dc hopping conductivity on the same footing as discussed above. (ii) The random network of impurity sites is replaced by a uniform media, a lattice of sites.

The basic $\psi(\vec{s}, t)$ is computed by considering a hop to an impurity on a site displaced by $\vec{s}$ in the presence of the other $N-1$ impurities distributed randomly on the lattice points. The resulting $\psi(\vec{s}, t)$ is configuration averaged over all the positions of the $N-1$ impurities. In a random walk on a random media one is again interested in a configuration average. However, for an n-step walk in the random media, the contribution is configuration averaged over the positions of the $N-n$ impurities. The difference in these averaging procedures is discussed in Appendix B of I.

II. IMPURITY CONDUCTION

The qualitative functional form for $\psi(\vec{s}, t)$ [for a $\psi(\vec{s}, t) = p(\vec{s})\psi(t)$] needed to reproduce the frequency dependence of the ac conductivity measured in impurity conduction was indicated in Sec. IV of I. In the following $\psi(\vec{s}, t)$ is calculated explicitly, starting from a basic description of known details of impurity hopping conduction.[3-16]

The system is specified as an n-type compensated semiconductor (e.g., Si, Ge) at a temperature low enough that all the carriers are frozen out on the donor sites. Transport takes place by an electron hopping from a neutral donor to a donor ionized by a compensating acceptor. In presence of the random electric field due to the ionized constituents, the energy levels will fluctuate and the individual hop is temperature activated (cf. Fig. 1 of PG[5]).

To determine $\psi(\vec{s}, t)$ one calculates the probability per unit time that in a time t between hops, the vacancy on an ionized donor (near the ionized acceptor) is displaced a vector distance $\vec{s}$ to a surrounding neutral donor. Fortunately, the statistical difficulties of a very similar problem were worked out by Thomas, Hopfield, and Augustyn-

iak[17]) (THA) in their consideration of the kinetics of radiative recombination of electrons trapped on donors with holes trapped on acceptors; both are randomly distributed. While they are concerned with transitions from a minority site to the surrounding majority sites, we consider transitions between an ionized majority site and the randomly placed neutral majority sites. To calculate $I(t)$, the *total* intensity of light emitted at time t due to the pair radiative recombination, they define $I(t) = -d\langle Q(t)\rangle/dt$, where $\langle Q(t)\rangle$ is the configuration averaged probability the electron (or vacancy) is still on the initial site at time t. Now, since $\langle Q(0)\rangle = 1$ and $\langle Q(\infty)\rangle = 0$, $I(t)$ is normalized to one and, therefore, from the defining relation it is apparent that $I(t) = \psi(t)$. The analog of $\psi(\vec{s}, t)$ in THA is $I_E(t)$, the intensity/unit energy at energy E and time t.

It is not surprising there should be an intimate connection between the pair fluorescence in semiconductors and the hopping transport (in the present formulation). The multiple path aspect[1] of the hopping has been accounted for and in (3) the diffusion is "reduced" to a function of the FT of the time spectrum of hops from a single site. In the fluorescence process the light given off in recombination is simply a signal that a hop has occurred. Moreover, the peak in the energy spectrum of the light emission at a given time t [$I_E(t)$] is a measure of the spatial separation of the pair of sites between which a hop most probably occurs at t [cf. Eqs. (18) and (20) in THA[17] and Figs. 4 and 6 in Ref. 18].

We now adopt the procedure in THA. Let $Q(t)$ be the probability that a vacancy on the donor at the origin at time $t = 0$ remains on the donor until time t. This probability can decrease in time via all the *parallel decay channels* for it to transfer to surrounding neutral donors:

$$\frac{dQ}{dt} = -Q\sum_j W(\vec{r}_j) \tag{8}$$

and

$$Q(t) = \exp\left(-\sum_j W(\vec{r}_j)t\right), \tag{9}$$

where $W(\vec{r})$ is the transition rate between donors separated by $\vec{r}$. In computing the configuration average of (9), one makes use of the well-known technique[17,19] for calculating the characteristic function of a sum of random variables

$$\langle Q(t)\rangle = \left\langle \exp\left(-t\sum_j W(\vec{r}_j)\right)\right\rangle$$

$$= \exp\left(-N_D\int d^3r\{1 - \exp[-W(\vec{r})t]\}\right), \tag{10}$$

with

$$\psi(t) = \frac{-d\langle Q(t)\rangle}{dt}. \tag{11}$$

One can formally rewrite (10) as

$$\ln\langle Q(t)\rangle = -N_D\int_0^\infty d\mu(1 - e^{-\mu t})F(\mu), \tag{12}$$

where

$$F(\mu) = \int d^3r\,\delta(\mu - W(\vec{r})) \tag{13}$$

is the spectrum of transition rates in the system.

It is obvious from (8) that the probability/unit time a hop occurs via one definite channel is

$$W(\vec{r}_1, t) = W(\vec{r}_1)Q(t)$$

$$= W(\vec{r}_1)e^{-W(\vec{r}_1)t}\exp\left(-t\sum_{j\neq1}W(\vec{r}_j)\right). \tag{14}$$

The distribution function $\psi(\vec{r}_1, t)$ is simply the configuration average of (14) holding the lattice position $\vec{r}_1$ fixed, multiplied by the probability that an impurity is on site $\vec{r}_1$,

$$\psi(\vec{r}_1, t) = N_D v W(\vec{r}_1)e^{-W(\vec{r}_1)t}\left\langle \exp\left(-t\sum_{j\neq1}W(\vec{r}_j)\right)\right\rangle, \tag{15}$$

where v is the lattice-cell volume. In the limit of a large number N of donors in the total volume V of the system ($N/V = N_D$, N, $V \to \infty$) the configuration averages over N or $N - 1$ donors are equivalent [cf. Eq. (18) in THA], so that

$$\psi(\vec{s}, t) = N_D v W(\vec{s})e^{-W(\vec{s})t}\langle Q(t)\rangle. \tag{16}$$

If we sum (16) over all $\vec{s}$,

$$\psi(t) = \sum_{\vec{s}}\psi(\vec{s}, t) = N_D v\sum_{\vec{s}}W(\vec{s})e^{-W(\vec{s})t}\langle Q(t)\rangle$$

$$= N_D\int d^3r\,W(\vec{r})e^{-W(\vec{r})t}\langle Q(t)\rangle, \tag{17}$$

which is equivalent to differentiating the expression for $\langle Q(t)\rangle$ in (10) and inserting the result into (11). As mentioned in Sec. I in the present paper, we will assume $\sigma_{rms}^2(\omega) \approx \sigma_{rms}^2(0)$. Thus, henceforth we consider only $\psi(t)$ in quantitative detail and reserve a fuller discussion of $\psi(\vec{s}, t)$ for the paper in Ref. 19 of I.

The form of (12) and (13) emphasizes the point, made in Sec. I, that the structure of the CTRW model allows one to focus on the transition rate as the main fluctuating quantity. In particular, the spectrum of transition rates determines $\psi(t)$ and hence the conductivity.

One significant difference between the THA treatment of pair fluorescence and impurity conduction is the form for $W(\vec{r})$. In THA,

$$W(r) = W_M e^{-r/R_d}, \tag{18}$$

a simple consequence of wave function "overlap," where R_d is half the effective Bohr radius a and W_M is a constant. In hopping between majority sites,

according to MA[3] [Eqs. (II14) and (II19) in MA],

$$W(\vec{r}) = W_0' \left(\frac{r}{R_d}\right)^{3/2} \Delta(r, \theta)$$

$$\times \exp\left(\frac{-r}{R_d}\right) \left[\exp\left(\frac{\Delta(r, \theta)}{\kappa T}\right) - 1\right]^{-1}$$

$$\simeq W_0' \left(\frac{r}{R_d}\right)^{3/2} \Delta(r, \theta) \exp\left(\frac{-r}{R_d}\right) \exp\left(\frac{-\Delta(r, \theta)}{\kappa T}\right) ,$$

$$(19)$$

where $\Delta(r, \theta)$ is the energy difference between the sites, and $\cos\theta = \hat{r} \cdot \hat{p}$, $\vec{p}$ is the displacement between the initial site nearest the ionized acceptor, and the acceptor (cf. Fig. 1, Ref. 15). For phonon absorption $\Delta > 0$ and for phonon emission $\Delta < 0$. The approximate form for $W(\vec{r})$ obtains for $\Delta/\kappa T \gg 1$ (which holds for the present application).

It is important to use (19) in the calculation because the energy fluctuation $\Delta(r, \theta)$, as well as the separation r, plays a role (at low T) in selecting the pairs of sites contributing to a specified range of transition rates. However, as will be shown in Sec. III A, the r, θ dependence of Δ are only important in the high-concentration case (where Δ is largest). In order to facilitate the calculation of $\psi(t)$ and its FT, (18) will be used for $W(r)$ with

$$W_M = W_0'(\bar{r}/R_d)^{3/2} |\Delta| e^{-\Delta/\kappa T} \qquad (20)$$

and $\bar{r}$, Δ taken at some appropriate mean value. With (20) the entire frequency dependence of $D(\omega)$ can be obtained in closed form, while with (19) detailed calculations have been performed in a more restricted frequency range [due to the necessity of choosing simple analytic forms for $\Delta(r, \theta)$ appropriate to either localized hopping or extended (dc) hopping]. In any case, details of the latter calculation will be contained in a forthcoming paper,[20] while the former results are in agreement with the measurements of PG at lower concentrations and/or higher temperature.

A. Calculation of $\psi(t)$

An analytic expression for $\psi(t)$ using (18) is derived in Appendix A and for large τ (the region of greatest interest for $0 < \omega/2\pi \leq 10^5$ Hz), the asymptotic form yields

$$\ln Q(\tau) = -(\tfrac{1}{3}\eta)\left[(\ln e^\gamma \tau)^3 + 3\zeta(2)\ln e^\gamma \tau + 2\zeta(3)\right] ,$$

$$(21)$$

with $Q(\tau) \equiv \langle Q(t) \rangle$, $\tau \equiv W_M t$, $\eta \equiv 4\pi N_D R_d^3$, $\gamma = 0.5772$, and $\zeta(s)$ is the Riemann ζ function.[21] In the new notation

$$\frac{\psi(t)}{W_M} = \frac{-dQ(\tau)}{d\tau} . \qquad (22)$$

For small τ,

$$\psi(t)/W_M = 2\eta - (\tfrac{1}{4}\eta + 4\eta^2)\tau + \cdots . \qquad (23)$$

The evaluation of $\psi(t)$ using (21)–(23) is an ex-

cellent agreement with the results for $I(t)$, obtained numerically, in Fig. 1 of THA (the ordinate scale in THA is inadvertently one power of ten too large). Adopting their $I(t)$ curves, we plot $\psi(t)/W_M$ vs τ in Fig. 2 with a range of values for η. For P donors in Si we use $R_d = 12$ Å (this value is based on the one calculated by MA in Ref. 3 and the alteration $a_D/a_{As} = 1.14$ required by Pollak in Ref. 15). Thus, e.g., $\eta = 10^{-4}$ corresponds to $N_D = 0.85 \times 10^{16}$ cm^{-3}.

The explicit calculation of $\psi(t)$ in Fig. 2 has qualitative features similar to the model $\psi(t)$ chosen in Sec. IV of I to fit the ac conductivity measurements of PG. Namely, a slow falloff (on the scale of $\bar{t} \equiv W_M \bar{t}$) with time. However, the $\psi(t)$ calculated with (21) and (22) is very dispersive in time; it falls off slower than exponential. This characteristic of $\psi(t)$ is conjectured to be a general property associated with hopping in amorphous systems. One consequence is that nth moment of $\psi(t)$ using (21) increases much faster (with increasing n) than the same quantity using Eq. (40) of I. This fact, in turn, implies that the CTRW process with the above $\psi(t)$ produces results (especially ac results) that could not be derived from a conventional master-equation approach to the hopping transport.[22]

One can understand the dispersive tail in $\psi(t)$ by considering a simple way to derive the main part of the analytic result in (21). The integrand in the exponent in (10) behaves as a unit step function:
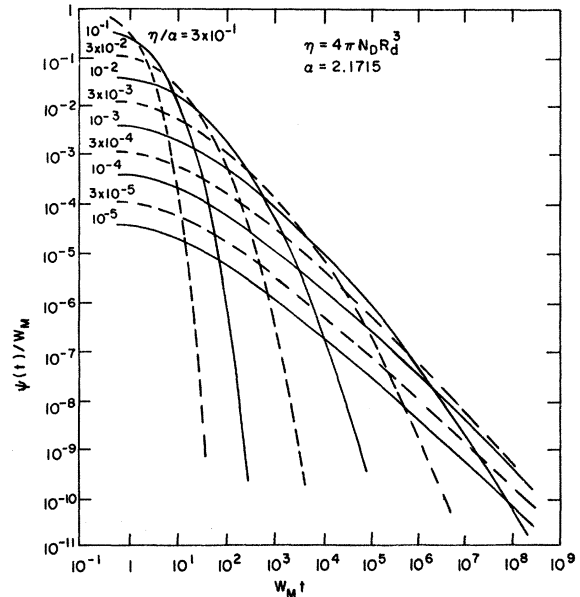
FIG. 2. Distribution function of random hopping times from a site $\psi(t)$ scaled by the maximum transition rate W_M, i.e., $W(\vec{r}) = W_M e^{-r/R_d}$, with $R_d = \tfrac{1}{2} \times$ (Bohr radius) and $W_M \propto \exp(-\Delta/\kappa T)$. The dimensionless $\psi(t)/W_M$ is a function of $\tau \equiv W_M t$ and $\eta \equiv 4\pi N_D R_d^3$. Characteristic of $\psi(t)/W_M$ for a disordered system is a slow (e.g., nonexponential) dependence on τ.

$$1 - \exp[- W(\vec{r})t] = \begin{cases} 1 , & W(\vec{r})t > 1 \\ 0 , & W(\vec{r})t < 1 . \end{cases} \quad (24)$$

Due to the general exponential dependence of $W(\vec{r})$ on $\vec{r}$, the transition from 1 to 0 in (24) is very rapid as a function of $\vec{r}$. With (18) for $W(\vec{r})$ and (24), the integral in (10) is simply

$$- 4\pi N_D \int_0^{r_\tau} r^2 \, dr = - \tfrac{4}{3}\pi N_D r_\tau^3 , \quad (25)$$

where

$$W(r_\tau)t = \tau e^{-r_\tau / R_d} = e^{-c} \simeq 1 \quad (26)$$

or

$$r_\tau = R_d \ln e^c \tau . \quad (27)$$

Inserting r_τ in (27) into (25) one obtains the leading term (for large τ) of (21) with the identification $c = \gamma$. The exact number e^γ was derived in Appendix A, but the main point is that $e^\gamma \sim 1$. The approximation in (24) is obviously an excellent one and is used to calculate $\langle Q(t) \rangle$[20] with more complicated forms for $W(\vec{r})$ [i.e., (19)], where simple analytic results, such as (21), are not possible. Thus, with the interpretation contained in (20) at any time t, the integral in (10) *sums up all the transition rates "down"* to $1/t$ [or ω, when the FT of $\psi(t)$ is considered]. The long tail in $\psi(t)$ is related to the absence of a truncation of the transition rate spectrum, or, at any t one can "find" a $W(r)$, such that $W(r)t \sim 1$ [the "volume" in (25) keeps increasing with t]. Stated in another way, if $F(\mu)$ in (12) were truncated,

$$\mu < \mu_{\min}: \quad F(\mu) = 0 , \quad (28)$$

then

$$\ln\langle Q(t) \rangle \xrightarrow[t > \mu_{\min}^{-1}]{} - N_D \int_{\mu_{\min}}^\infty F(\mu) \, d\mu \quad (29)$$

or

$$\psi(t) \xrightarrow[t > \mu_{\min}^{-1}]{} N_D \int_{\mu_{\min}}^\infty d\mu \, e^{-\mu t} \, \mu F(\mu) \sim e^{-\mu_{\min} t} . \quad (30)$$

Therefore, the highly dispersive nature of $\psi(t)$ in disordered systems is related to the shape of $F(\mu)$ for $\mu \sim 0$. In particular, the lack of a "cutoff" in $F(\mu)$ for μ in a finite neighborhood of the origin.

Qualitatively, the steeper the time variation of $\psi(t)$, the slower the ω dependence of $D(\omega)$. Hence, one can already understand some features of the experimental behavior of the ac conductivity (Figs. 5 and 6 in PG) by examining the $\psi(t)$ curves in Fig. 2. Since W_M increases with increasing temperature [Eq. (20)], a fixed value of t (e.g., corresponding to a fixed ω^{-1}) slides to the right on the τ abcissa, i.e., it moves to a region where $\psi(t)$ has a steeper t dependence. Therefore, for a

given ω, $D(\omega)$ has decreasing ω dependence with increasing temperature (cf. Fig. 5, PG). Similar results hold for increasing N_D [at *fixed* (higher) T] leading to lower ω dependence of $D(\omega)$ (cf. Fig. 6, PG). The latter conclusion is somewhat complicated by the fact that increasing N_D not only increases η but also changes Δ in W_M (i.e., τ is not a constant for a fixed t), but this is alleviated at higher T, where changes in Δ are less important. These ω, T, and N_D dependences of $D(\omega)$ will be exhibited in detail after computation of the FT of $\psi(t)$.

B. $D(\omega)$ and the Fourier Transform of $\psi(t)$

It is expedient to express the FT of $\psi(t)$ in terms of $Q(\tau)$. Inserting (22) into (2) and integrating by parts,

$$\tilde{\psi}(i\omega) = 1 - i\Omega \tilde{Q}(\Omega) , \quad (31)$$

where $\Omega \equiv \omega/W_0$ [$W_0 = W_M e^\gamma$, for the model using (18)] and

$$\tilde{Q}(\Omega) = \int_0^\infty d\tau \, e^{-i\Omega\tau} Q(\tau)$$

$$= \int_0^\infty d\tau \exp\left(-i\Omega\tau - N_D \int d^3 r \right.$$

$$\left. \times \{1 - \exp[-\tau W(\vec{r})/W_0]\}\right) . \quad (32)$$

Inserting (31) in (3) one has an even simpler form for the frequency-dependent diffusion constant:

$$\bar{D}(\Omega) \equiv D(\omega)/\tfrac{1}{6}\sigma_{\text{rms}}^2 W_0 = [\tilde{Q}(\Omega)]^{-1} - i\Omega . \quad (33)$$

The frequency range of interest is such that $\Omega \ll 1$ [from PG, Eq. (13a), W_0' in (20) is $0.82 \times 10^{12}/$ meV sec; Pollak[23] used a $|\Delta|/\kappa \simeq 10 \,^\circ$K]. In that case (as shown in Appendix B),

$$\tilde{Q}(\Omega) \simeq \int_1^\infty d\tau \, e^{-i\Omega\tau} Q(\tau)$$

$$= \int_0^\infty dx \exp[x - i\Omega e^x - \eta\xi(x)] , \quad (34)$$

where $x = \ln\tau$ and $\xi(x)$ is, generally, a rational function of x, e.g., from (25) and (27), $\xi(x) = \tfrac{1}{3} x^3$. The integral in (34) can be developed into an asymptotic series by applying the method of steepest descent.[24] The leading term in the series is obtained from the contribution at the saddle point and is worked out in detail in Appendix B for the model using (18) for $W(\vec{r})$. The final results can be summarized as

$$\bar{D}(\Omega) = e^{-\Phi(z_0)} [-\Phi''(z_0)/2\pi]^{1/2} - i\Omega , \quad (35)$$

with

$$\Phi(z_0) = z_0 - (\tfrac{1}{3}\eta)z_0^3 - 1 + \eta z_0^2 , \quad (36)$$

$$- \Phi''(z_0) = 1 + 2\eta z_0 - \eta z_0^2 , \quad (37)$$

and

$$z_0 = x_0(\Omega) + iy_0(\Omega) . \quad (38)$$

In Fig. 3 we plot $x_0(\Omega)$ and $y_0(\Omega)$ for $\eta = 6 \times 10^{-3}$ and
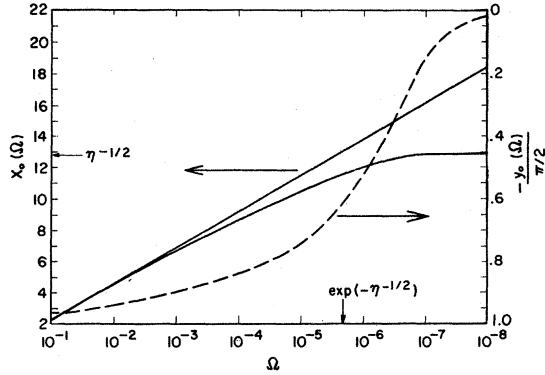
FIG. 3. Real x_0 (solid line), and imaginary y_0 (dashed line) part of the saddle point z_0, used in the asymptotic expansion of the FT of the hopping time distribution $\psi(t)$, vs $\Omega \equiv \omega/W_M$. The solid straight line is $-\ln\Omega$. z_0 is an explicit function of $\eta \equiv 4\pi N_D R_d^3$ as well as Ω/η. The above plot is for $\eta = 6 \times 10^{-3}$. The limiting value $\eta^{-1/2}$ for $x_0(\Omega \to 0)$ and $\exp(-\eta^{-1/2})$, the value of Ω characterizing the transition to dc behavior for $\sigma(\omega)$, is indicated above.

also, for comparison, the straight line $-\ln\Omega$. Note that $x_0 \simeq -\ln\Omega$ and $1 + y_0/\frac{1}{2}\pi \propto -\ln\Omega$ for the region $-\ln\Omega < \eta^{-1/2}$; this functional dependence leads to

$$\overline{D}(\Omega) \simeq A\Omega^s \tag{39}$$

or

$$D(\omega) \simeq \frac{1}{6}\sigma_{rms}^2 A(\overline{W}_0 e^{-\Delta/\kappa T})^{1-s}\omega^s , \tag{40}$$

$$\overline{W}_0 = e^\gamma W_0'(\overline{r}/R_d)^{3/2}|\Delta| , \tag{41}$$

where A is a complex constant and s is a constant in this frequency region (to be discussed below).

In the limit $\Omega \to 0$,

$$\tilde{Q}(0) = \int_0^\infty dx \exp(x - \frac{1}{3}\eta x^3) = \pi\eta^{-1/3}\text{Hi}(\eta^{-1/3})$$

$$\sim (\pi\eta^{-1/2})^{1/2}\exp(\frac{2}{3}\eta^{-1/2}) , \tag{42}$$

using formula 10.4.44 of Ref. 21 for the definition of Hi(z) (a type of Airy function) and 10.4.90 for the asymptotic form (for large $\eta^{-1/2}$). The asymptotic result for the exact $\tilde{Q}(0)$ in (42) agrees completely with the asymptotic result for $\Omega \to 0$ using (B15)–(B17), (B20), and (B21). Substituting (42) into (33), one has, for the dc conductivity,

$$\sigma(0) = \frac{N_A e^2}{\kappa T} D(0)$$

$$= \frac{N_A e^2}{\kappa T}\frac{\sigma_{rms}^2}{6\sqrt{\pi}}\overline{W}_0 e^{-\Delta/\kappa T}\eta^{1/4}\exp(-\frac{2}{3}\eta^{-1/2}) . \tag{43}$$

The dominant majority concentration dependence of $\sigma(0)$ in (43),

$$\exp(-\frac{2}{3}\eta^{-1/2}) = \exp[-2(r_D/3R_d)^{3/2}] , \tag{44}$$

is the same as found by MA.[3] In the MA theory the problem of calculating the dc hopping resistivity is

reduced to solving for the resistance of a network of randomly placed junctions joined by resistors with a prescribed distribution in value. MA chose parallel current paths with a string of resistors corresponding to nearest or next-nearest intersite hops. All other dc hopping conductivity calculations have differed in the details of constructing the current paths, but have retained the basic network model. In the present formulation a result similar to the MA one for $\sigma(0)$ was derived without invoking a network of resistors or specifying the proximity of the intersite hops. The final expression in (43) is based on the use of a simple form for the transition rate $W(r)$. A more complete form for $W(r)$ [i.e., (19)] will produce modifications in (43).[20] In Ref. 14, percolation-threshold criteria have been used to determine the effective current paths. In effect, a truncation of the type in (28). With this approach they find that $-\ln\sigma(0) \propto r_D$. For the small range in N_D considered in Sec. III we find (43) to be satisfactory. To test the different dependencies on N_D in $\sigma(0)$ ($r_D/r_D^{3/2} \propto N_D^{1/6}$), one would need a much larger range of N_D (for the low-compensated system).

The complete numerical results for $\overline{D}(\Omega)$ [Eq. (33)] based on Eqs. (35)–(37) for two values of N_D are shown in Fig. 4 ($\eta = 6 \times 10^{-3}$) and Fig. 5 ($\eta = 2.22 \times 10^{-4}$). The general features of both plots are (i) not only do the curves for $\overline{D}$ show the complete frequency dependence of $\text{Re}\overline{D}$ including the transition to dc, but a complete description of $\text{Im}\overline{D}$ including the transition of $\text{Im}\overline{D}/\omega \to$ const. $\propto \epsilon_0$; (ii) a Ω^s dependence at the higher values of Ω with a constant $s \sim 0.6$ (for three decases of Ω) in Fig.
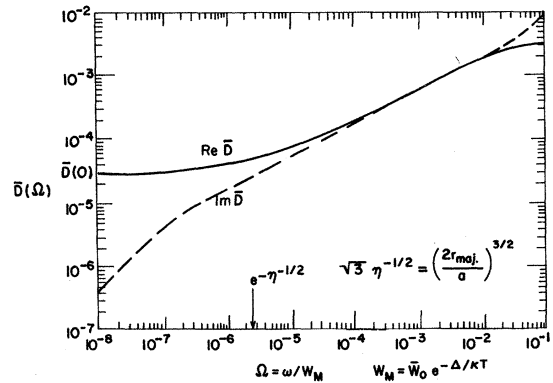
FIG. 4. Real $\mathfrak{R}\overline{D}$ (solid line) and imaginary $\mathfrak{I}\overline{D}$ (dashed line) parts of the dimensionless diffusion constant $\overline{D}(\Omega)$ $\equiv D(\omega)/(\frac{1}{6}\sigma_{rms}^2 e^\gamma W_M)$ with $\gamma = 0.5772$; $\Omega \equiv \omega/W_M e^\gamma$, with W_M defined in Eq. (20). The plot is for $\eta \equiv 4\pi N_D R_d^3 = 6 \times 10^{-3}$, where $R_d = \frac{1}{2}a$; a is the effective Bohr radius. In the above, $r_{maj} \equiv r_D = (\frac{4}{3}\pi N_D)^{-1/3}$. Indicated in the plot are the values for $\overline{D}(0) \simeq \eta^{1/4}\exp(-\frac{2}{3}\eta^{-1/2})/\sqrt{\pi}$ and $\Omega_c \simeq \exp(-\eta^{-1/2})$, the frequency characterizing the transition to dc (cf. Appendix B 2).
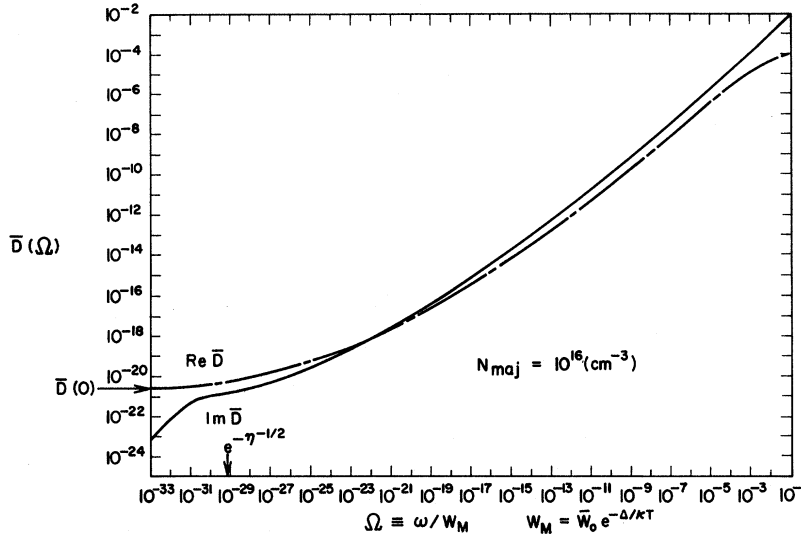
FIG. 5. Real $\Re \bar{D}$ (dot-dashed line) and imaginary $\Im \bar{D}$ (solid line) parts of the dimensionless diffusion constant $\bar{D}(\Omega) \equiv D(\omega)/(\frac{1}{6}\sigma_{rms}^2 e^\gamma W_M)$, with $\gamma = 0.5772$; $\Omega \equiv \omega/W_M e^\gamma$, with W_M defined in Eq. (20). The plot is for $\eta \equiv 4\pi N_D R_d^3 = 2.22 \times 10^{-4}$, where $R_d = \frac{1}{2}a$; a is the effective Bohr radius. The value $N_{maj} = N_D = 10^{16}$ cm^{-3} corresponds to $R_d = 12$ Å. Indicated in the plot are the values for $\bar{D}(0)$ $\simeq \eta^{1/4} \exp(-\frac{2}{3}\eta^{-1/2})/\sqrt{\pi}$ and Ω_c $\simeq \exp(-\eta^{-1/2})$, the frequency characterizing the transition to dc (cf. Appendix B 2).

4 and $s \sim 0.8$ (for 15 decades of Ω) in Fig. 5; (iii) a transition from the Ω^s dependence to dc behavior in the neighborhood of a characteristic frequency $\Omega_c = \exp(-\eta^{-1/2})$ (cf. the last part of Appendix B 2 for a fuller discussion of Ω_c); (iv) a limiting value $\bar{D}(0)$ yielding a dc conductivity similar to that derived by MA[3]; (v) for fixed ω, $\bar{D}$ tends to dc with increasing temperature, i.e., even with fixed ω, the dimensionless frequency Ω decreases with increasing T; (vi) as indicated in (40) for $D(\omega)$, one has larger temperature dependence directly correlated with lower frequency dependence. The N_D dependence of the frequency dependence of D depends on the value of Δ which, in general, is $\propto N_D^{1/3}$. Thus, the N_D dependence is best discussed in the context of the detailed comparison with experiment in Sec. III.

III. COMPARISON WITH EXPERIMENT

The experimental data that we will compare with theory (Figs. 4 and 5) are contained in Figs. 3, 5, and 6 in PG. Parts of these figures pertinent to our discussion will be reproduced in this section. The portions of the $\bar{D}(\Omega)$ curves in Figs. 4 and 5 that are relevant to the PG results depend on the range of Ω. Now PG measured the conductivity for $10^2 < \omega/2\pi < 10^5$ Hz. With the value $W_0' = 0.82 \times 10^{12}/$ meV sec, already quoted in the text, a typical value for $\bar{W}_0$, in (41), is $\bar{W}_0 \sim 10^{13}$–10^{14} sec^{-1}, depending on $\bar{r}$, Δ. Thus, the smallest value for Ω (at high T, $\Omega \sim \omega/\bar{W}_0$) corresponding to the ac range of PG is $\Omega_{min} \sim 10^{-12}$ (of course, for the dc case $\Omega = 0$). Inspection of the Ω scale in Figs. 4 and 5 shows that a value of $\Omega_{min} \sim 10^{-12}$ covers the entire range in Fig. 4, including the transition to dc behavior, while in Fig. 5, $\bar{D}(\Omega) \propto \Omega^{0.8}$ for $\Omega > \Omega_{min}$. This is in qualitative agreement with Figs. 5 and 6 in PG.

For the samples with $N_D \gtrsim 10^{17}$ cm^{-3}, PG observed a gradual transition from $\text{Re}\sigma(\omega) \propto \omega^{0.9}$ to $\text{Re}\sigma(\omega)$ $\propto \sigma(0)$, at each fixed value of ω, with increasing T. For samples with $N_D \sim 10^{16}$ cm^{-3}, the frequency dependence $\sigma(\omega) \propto \omega^s$, $s \simeq 0.8$, persisted with increasing T until at $T \gtrsim 15$ °K the electrons on the P donors are ionized into the conduction band of the host Si (this will be more fully discussed below). The only measurements of *dc impurity conduction* in PG are for the samples with $N_D > 10^{17}$ cm^{-3}.

Thus for the samples with $N_D \gtrsim 10^{17}$ cm^{-3} and for $N_D \sim 10^{16}$ cm^{-3}, there are two different qualitative dependences on ω, T for the experimental range of these variables used by PG. We shall refer to the former as "high" concentration and the latter as "low" concentration. For all these samples $N_A = 0.8 \times 10^{15}$ cm^{-3}. The theory pertaining to each concentration case is in Figs. 4 and 5, respectively, and will be discussed separately in Secs. III A and III B. Before this analysis, we want to point out that these theoretical results for $D(\omega)$ include both the $\text{Re}D(\omega)$ and $\text{Im}D(\omega)$ and although the comparison with experiment, in the present paper, deals mainly with $\text{Re}D(\omega)$, we would like to make the following observations concerning $\text{Im}D(\omega)$. Figure 3 of PG is a log-log plot of both the Re and Im parts of $\sigma(\omega)$ vs $\omega/2\pi$ for a sample with $N_D = 1.4 \times 10^{16}$ cm^{-3}. The plot is a series of straight lines with the slopes varying slowly with temperature; i.e., $\text{Re}\sigma$, $\text{Im}\sigma \propto \omega^{s(T)}$, where $s(T)$ is equal to 0.79 at 3 °K and 0.74 at 12 °K. At each temperature T, this slope s is an average over three decades of frequency (s is also a very slowly varying function of ω). A *convenient way* to show the relation between $\text{Re}\sigma$ and $\text{Im}\sigma$ and also demonstrate the ω and T variation in s is to make use of the Kramers–Kronig relation for *this frequency range*. This relation [quoted in PG, Eq. (2)] is

TABLE I. Comparison of real and imaginary parts of σ.

	Experiment[a]			Theory[b]	
$s = (2/\pi)\,\tan^{-1}(\mathrm{Im}\sigma/\mathrm{Re}\sigma)$	$\omega/2\pi$ (Hz)	T (°K)	$s = (2/\pi)\,\tan^{-1}(\mathrm{Im}\sigma/\mathrm{Re}\sigma)$	$\Omega\ (=\omega/\overline{W}_0\,e^{-\Delta/kT})$	
0.81	10^5	3	0.83	2×10^{-6}	
0.81	10^2	3	0.82	4×10^{-9}	
0.79	10^5	4.2	0.82	10^{-9}	
0.79	10^2	4.2	0.81	4×10^{-11}	
0.78	10^5	8	0.80	2×10^{-12}	
0.75	10^2	8	0.78	10^{-13}	
0.76	10^5	12	0.76	10^{-14}	
0.72	10^2	12	0.73	10^{-15}	

[a]Figure 3 in PG, see text.　　　　　　　　　　　[b]From Fig. 5 in text.

$$\mathrm{Im}(\sigma)/\mathrm{Re}(\sigma) = \tan(\tfrac{1}{2}s\pi) \ . \qquad (45)$$

{We have not made the separation $\sigma_{ac} \equiv \sigma - \sigma_{dc}$ [PG, Eq. (1)] since this is unnecessary.} Thus, if we compare the experimental and theoretical value of

$$s = (2/\pi)\,\tan^{-1}(\mathrm{Im}\sigma/\mathrm{Re}\sigma) \ , \qquad (46)$$

we simultaneously consider the ratio of $\mathrm{Im}\sigma$ to $\mathrm{Re}\sigma$ and the "point-wise" variation of s with ω and T. On the left-hand side of Table I we list the values of s [in Eq. (46)] for a range of ω and T from Fig. 3 of PG and on the right-hand side of Table I the theoretical value for the same quantity s as a function of Ω (from Fig. 5). The near equality for the two columns of s values indicates that the experimental and theoretical value of $\mathrm{Im}\sigma/\mathrm{Re}\sigma$ are in good agreement. In addition, it shows that the asymptotic calculation of $D(\omega)$ (cf. Appendix B) preserves the Kramers–Kronig relation (cf. Appendix A of I).[25] The trend towards smaller s with increasing T and decreasing ω in both columns of Table I are also in agreement. In Sec. III B we show that the temperature range 3–4.2 °K corresponds to $\Omega \sim 10^{-9}$ so that the theoretical value $s = 0.82$–0.81 corresponds well with $s = 0.81$–0.79 in the left-hand column of Table I. As analyzed in Sec. III B for $T > 6$ °K we conjecture that a new hopping channel comes in [based on the temperature dependence of $D(\omega)$] and the comparison in Table I at the higher T is more complicated. We reserve discussion of this feature at higher T until Sec. III B. For a high-concentration case we compare $\mathrm{Re}\sigma$ and $\mathrm{Im}\sigma$ in PG, Figs. 6(a) and 6(b) for the sample with $N_D = 1.1 \times 10^{17}$ cm^{-3}. For this case we restrict the comparison to the higher-temperature range $T > 4$ °K (this restriction is fully detailed in Sec. III A). In Fig. 4, the $\overline{D}(\Omega)$ curves are computed for $N_D = 2.7 \times 10^{17}$ cm^{-3}, which is a factor 2.45 larger than the concentration of the sample under consideration with 1.1×10^{17} cm^{-3}. Thus, the values of s in Fig. 4 can be expected to be somewhat smaller than the experimental values. Further, in Fig. 4 the dependence, $\mathrm{Re}\overline{D}$, $\mathrm{Im}\overline{D}$ $\propto \Omega^s$ ($s \simeq 0.6$), is only over an Ω range $\gtrsim 2$ decades,

hence the relation in (45) is not as useful. In Figs. 6(a) and 6(b) (of PG) at 4.2 °K: the ratio $\mathrm{Im}\sigma/\mathrm{Re}\sigma$ varies from 1.83 at 10^5 Hz to 1.2 at 10^2 Hz and at 6.2 °K: $\mathrm{Im}\sigma/\mathrm{Re}\sigma = 1.6$ at 10^5 Hz, 1.25 at 10^4 Hz, and 0.32 at 10^2 Hz! {A ratio $\mathrm{Im}\sigma/\mathrm{Re}\sigma = 1.4$ corresponds to $s = 0.6$ [from (46)].} This is in good qualitative agreement with Fig. 4, especially the fact that the curves cross and $\mathrm{Re}\sigma > \mathrm{Im}\sigma$ at lower Ω (decreasing ω, increasing T). Thus, for both concentration cases the ratio $\mathrm{Im}\sigma/\mathrm{Re}\sigma$, derived from Figs. 4 and 5, compares well with the measurements of PG.

A. High Concentration: $N_D > 10^{17}$ cm^{-3}

For the high-concentration samples, the activation energy Δ associated with the dc impurity conduction is $\Delta \sim 5$–6 meV. Figure 1 in PG and Fig. 1 in Ref. 15 are pictorial representations of the origin of the activation energy (the Mott–Conwell model) for low-compensated semiconductors. In general $\Delta \propto N_D^{1/3}$. MA[3] have derived the following expression for low-compensated semiconductors:

$$\Delta = \frac{e^2}{\epsilon}\left(\frac{1}{r_D} - \frac{1.35}{r_A}\right)$$

$$= \frac{e^2}{\epsilon}\,(\tfrac{4}{3}\pi)^{1/3}\,N_D^{1/3}(1 - 1.35K^{1/3}) \ , \qquad (47)$$

where $K = N_A/N_D$ and ϵ is the host dielectric constant [the form of (47) is valid for $K < 0.03$]. The larger the concentration N_D the shorter the distance between the acceptor ion and the nearest compensated donor and thus the further into the Coulomb well of the acceptor ion. The K-dependent "correction" in (47) is due to the presence of other nearby acceptor ions.

At finite frequencies and low temperatures the ac hopping is localized [cf. (27) and PG] and the effective activation energy $\Delta_{eff} < \Delta$. As ω decreases or T increases hops occur over larger distances and $\Delta_{eff} \rightarrow \Delta$. Thus, for ac hopping Δ_{eff} is ω dependent and at low temperatures, the smaller Δ_{eff} is an important feature. At higher concentrations, Δ is not only larger in magnitude, but the
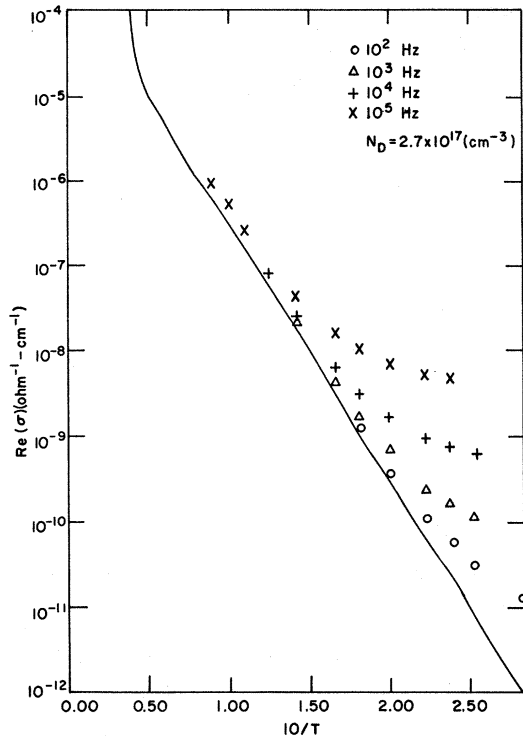
FIG. 6. Real part of the conductivity $\mathrm{Re}\sigma(\omega)$ vs $10/T$, replotted from Fig. 5 of Pollak and Geballe, Ref. 5 (cf. also Ref. 26) for $10/T < 2.85$. The dc impurity conduction $\sigma(0)$ is the solid curve, the other values of $\mathrm{Re}\sigma(\omega)$ correspond to the frequencies, $\omega/2\pi$, indicated above.

energy differences between the donor sites (which give rise to Δ) vary more rapidly with donor spatial separation. At lower concentration all intersite distances are increased and the donors are typically in regions of slowly varying potentials. One can thus conclude that the use of (18) with a mean Δ instead of (19) is inadequate at high concentration. The use of (19) would give rise an additional ω-dependent term of the form $\exp\{-\eta^{\alpha}[\ln(\overline{W}_0/\omega)]^{\beta}/\kappa T\}$, where α and β depend on the functional form of $\Delta(r, \theta)$.[19] The consequences of this additional term are diminished at higher T, lower N_D, and lower ω. For this reason we compare the theoretical results in Fig. 4, obtained with the use of (18) to the *higher* T measurements of PG on the high-concentration sample, in Fig. 5 of PG.[26]

This temperature region ($T > 3.5$ °K) includes the extremely interesting measurements of the transition to dc, for each fixed frequency, as a function of increasing T. In Fig. 6 we replot the data[26] corresponding to $10/T < 2.85$ to show all the points we use in our analysis. The transcription has been accomplished with an Edwin digitizer and the solid line in Fig. 6 is a result of the plotter connecting the data points of the dc conductivity, i.e., a "best" straight line has not been fitted to the dc

data. In Fig. 7 we plot $D(\omega)$ vs $10/T$ derived from (5) and the values of $\sigma(\omega)$ in Fig. 6. The solid line is $D(0)$ and for $1.6 < 10/T < 2.85$ the data points lie on a straight line (the lower dashed line) with a slope corresponding to $\Delta = 6.1$ meV. For $0.8 < 10/T < 1.6$ the dc points lie on a line with slightly larger slope ($\sim 1\%$ larger). We have not fitted the points to one straight line but simply use $\Delta = 6.1$ meV. The sharp rise in $D(0)$ at the upper end of the temperature range results from donor ionization into the conduction band (cf. PG and discussion in Sec. III B). In Table II we list the values of

$$\overline{D}(0)_{\mathrm{expt}} = D(0)/\tfrac{1}{6}\,\sigma_{\mathrm{rms}}^2\overline{W}_0\exp(-\Delta_{\mathrm{expt}}/\kappa T) \qquad (48)$$

derived from the individual data points,[26] with $\sigma_{\mathrm{rms}} = 0.95 r_D$,[27] $\overline{W}_0$ in (41), and $e^{\gamma}W_0' = 1.46 \times 10^{12}$ sec^{-1}, $R_d = 12$ Å, $\overline{r} = r_D$. The comparison is made with

$$\overline{D}(0)_{\mathrm{th}} = \eta^{1/4}\exp(-\tfrac{2}{3}\eta^{-1/2})/\pi^{1/2} . \qquad (49)$$

For the sample with $N_D = 2.7 \times 10^{17}$ cm^{-3} ($\eta = 6 \times 10^{-3}$) the left-hand column of $\overline{D}(0)_{\mathrm{expt}}$ shows a nearly constant value while a slow increase with increasing T is observed for the right-hand column of $\overline{D}(0)_{\mathrm{expt}}$. The latter behavior just reflects the need for a slightly larger Δ_{expt} for this tempera-
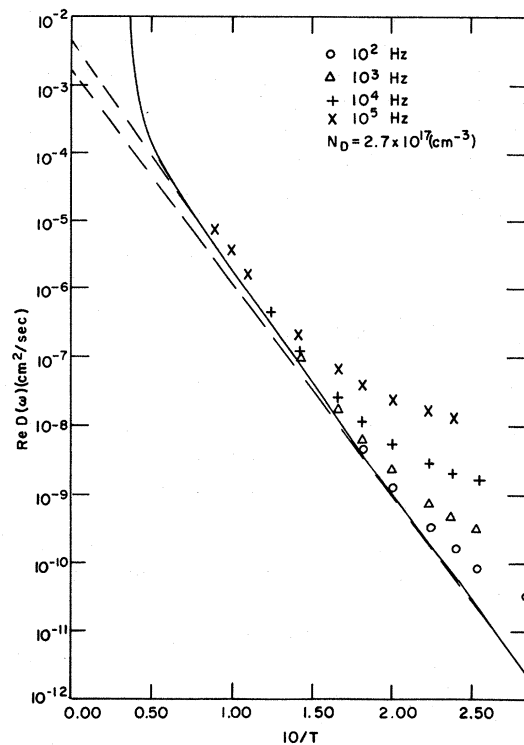
FIG. 7. Real part of the diffusion constant $\mathrm{Re}D(\omega)$ [derived from the measured values of $\mathrm{Re}\sigma(\omega)$ in Fig. 6 with the relation $\mathrm{Re}D(\omega)(\mathrm{cm}^2/\mathrm{sec}) = (0.6723T)\,\mathrm{Re}\sigma(\omega)\,(\Omega^{-1}\mathrm{cm}^{-1})$] vs $10/T$. $D(0)$ is the solid curve and the dashed lines are explained in the text [above Eq. (48)].

TABLE II. The dc impurity conduction in n-type Si.

N_D, $\bar{W}_0$ (cm^{-3}) (sec^{-1})	10/T	$\bar{D}(0)_{expt}$ ×10^5	10/T	$\bar{D}(0)_{expt}$ ×10^5	$\bar{D}(0)_{th}$ ×10^5	Δ_{expt}	Δ (MA) meV	Δ (ESY) meV
2.7×10^{17}	2.62	2.95	1.67	4.12	2.87	6.1	9.65	6.85
	2.51	3.36	1.43	4.89				
2.3×10^{14}	2.39	3.54	1.25	5.43				
	2.24	3.25	1.11	5.69				
	2.01	3.61	0.92	7.01				
	1.82	3.33	0.77	6.70				
$1.1 \times 10^{17\,a}$	2.3	1.79×10^{-2}			1.75×10^{-2}	5.0	6.55	4.98
3.36×10^{14}	1.6	2.24×10^{-2}						

[a] M. Pollak and T. Geballe (unpublished data).

ture range, discussed above (cf. Fig. 7). The average of the former $\bar{D}(0)_{expt}$ values is 3.34×10^{-5} which is a factor of 1.17 larger than $\bar{D}(0)_{th}$. The agreement is good. Also contained in Table II is unpublished data of PG[26] for a sample with N_D $= 1.1 \times 10^{17}$ cm^{-3} ($\eta = 2.44 \times 10^{-3}$). The individual data points were not shown on the $\sigma(\omega)$-vs-10/T plot,[26] just a straight line with a slope corresponding to $\Delta_{expt} = 5.0$ meV. Two 10/T points were chosen arbitrarily and the associated $\bar{D}(0)_{expt}$ evaluated as in (48), with the appropriate constants. The average $\bar{D}(0)_{expt}$ is 2.02×10^{-7}, a factor of 1.15 larger than $\bar{D}(0)_{th}$. Again, the agreement is good and indicates the N_D dependence of (49) (at least for this concentration range in Si) is very satisfactory [cf. the discussion following (44)].

The right-hand columns of Table II are various activation energies. The values for Δ_{expt} were already discussed; Δ (MA) is evaluated from (47) with $e^2/\epsilon = 1.15 \times 10^{-5}$ cm meV (cf. Fig. 2, Ref. 15). A better agreement with Δ_{expt} is obtained with an expression for the activation energy in low-compensated semiconductors recently derived by Efros, Shklovskii, and Yanchev[28] (ESY):

$$\Delta = (e^2/\epsilon)(0.99)N_D^{1/3}(1 - 0.43\nu K^{1/4}) , \qquad (50)$$

where $\nu \sim 0.7$. ESY take into account the possibility of a second unoccupied donor in the vicinity of the acceptor ion, which influences the energy of the first one.

In Fig. 1 we plot $\bar{D}(\Omega)$ vs Ω; the solid line is the theoretical curve for Re$\bar{D}(\Omega)$ reproduced from Fig. 4. All the points are obtained from Fig. 7 by dividing each value of Re$D(\omega)$ by the same factor as in the denominator on the right-hand side of (48), the corresponding Ω is obtained by computing $\omega/$ $\bar{W}_0 \exp(- \Delta_{expt}/\kappa T)$, with $\Delta_{expt} = 6.1$ meV. The most striking aspect of the Ω plot in Fig. 1 is that the four separate curves, each with a fixed value of $\omega/2\pi$, in Fig. 7 now lie on a *universal* curve. In other words, Fig. 1 is a *simultaneous display of both the frequency and temperature dependence* of the ac diffusion. In Fig. 7 each curve, for

fixed ω, "merged" with the dc at some temperature $T_{tr}(\omega)$, a function of the particular ω. Replotted in Fig. 1 the transition to dc for all the curves in Fig. 7 is characterized by one value of Ω, which is designated $\Omega_c \equiv \exp(-\eta^{-1/2})$ [cf. discussion following Eq. (B22)]. The spread in limiting values of $\bar{D}(0)$ for the four frequencies in Fig. 1 is again a reflection of the need for a slightly larger Δ_{expt} for 10/$T < 1.6$ (cf. Table II). The three highest-temperature points for $\omega/2\pi = 10^5$ Hz present a special problem. The experimental error, at this frequency and in this temperature range (corresponding to the largest dc loss: $\sigma \sim 5$ $\times 10^{-7}$ Ω^{-1} cm^{-1}), is expected to be large ($\sim 30\%$).[23] These points have been reduced by 1.3 in Fig. 1, but still lie outside the limiting values of the other frequencies. This feature aside, the agreement with the theoretical curve is quite good (the maximum deviation is ~ 1.5). In this regard, it should be stressed that there are no "fitted" parameters in Fig. 1. The basic parameter Δ_{expt} needed to reduce the *ac data* is determined in an independent measurement of the *dc* impurity conduction.

B. Low Concentration: $N_D \sim 10^{16}$ cm^{-3}

At low concentration, following our discussion in Sec. III A, the approximation in (18) of using an average activation energy Δ is expected to be a reasonable one. Therefore, in Fig. 8, all the data corresponding to one concentration, $N_D = 1.2 \times 10^{16}$ cm^{-3}, from Fig. 6(a) in PG are reproduced. Again, using (5) we plot Re$D(\omega)$, derived from the points in Fig. 8, vs 10/T in Fig. 9. In addition to the data points there are a number of solid and dashed lines in Fig. 9, which represent our analysis of the temperature dependence of Re$D(\omega)$. At the high-temperature end ($T > 15$ °K) the near vertical dashed line in Fig. 9 clearly shows the ionization of the P donors into the conduction band of Si. The line was drawn to pass through the two points with the highest values of Re$D(\omega)$ for $\omega/2\pi = 10^2$, 10^3 Hz, respectively. The slope of the line corresponds to an activation energy of 42 meV. The ground-state
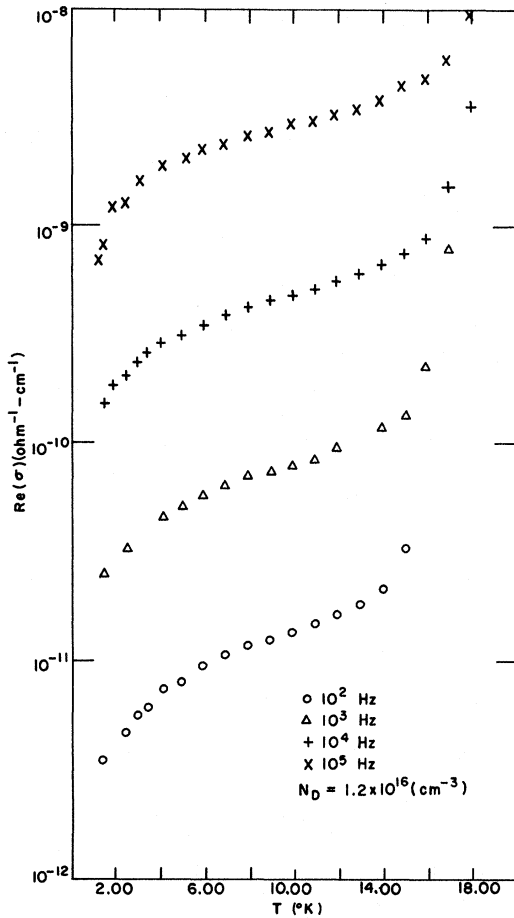
FIG. 8. Real part of the conductivity $\mathrm{Re}\sigma(\omega)$ vs $T(^\circ\mathrm{K})$, replotted from Fig. 6(a) of Pollak and Geballe, Ref. 5, for one value of the Donor concentration $N_D = 1.2 \times 10^{16}$ cm^{-3}. The values of $\mathrm{Re}\sigma(\omega)$ correspond to the frequencies $\omega/2\pi$, indicated above.

energy for a P donor[29] in Si is $\epsilon_d = 45$ meV, where ϵ_d is measured from the bottom of the conduction band. The temperature dependence of the density of electrons in the conduction band of an n-type semiconductor, at low T, is given by[30]

$$n = (K^{-1} - 1)\,(m_e \kappa T/2\pi\hbar^2)^{3/2} \exp(-\epsilon_d/\kappa T) \qquad (51)$$

for a *partially compensated* semiconductor [for $K = 0$, the activation energy for n is $\frac{1}{2}\epsilon_d$[30]]. Thus, (51) accounts for the temperature dependence of $D(\omega) = \kappa T\sigma(\omega)/N_A e^2$ in this temperature region; also, note that the transition into the conduction band wipes out the frequency dependence of $\mathrm{Re}D(\omega)$. The latter behavior is analogous to the transition, shown in Fig. 1 for the high-concentration sample, from ω-dependent *localized* hopping to ω-independent *delocalized* impurity conduction.

The four parallel dashed lines pass through the low-temperature points and it is clear that the strong departure from these lines when $10/T > 1.7$

cannot be accounted for by the approach to the nearly vertical dashed line discussed above. There is an "intermediate-" temperature behavior of $\mathrm{Re}D(\omega)$ between the donor ionization at one end and the low-temperature small (apparent) activation behavior at the other end. The four solid lines in Fig. 9 pass through points obtained by subtracting the value of the extrapolated low-temperature line (for each ω) from the respective data points (at the same ω) in this intermediate region. The lines are parallel and suggest an additional activation energy in the analysis of the temperature dependence of $\mathrm{Re}D(\omega)$.

Except for the *ionization region*, at each fixed T the frequency dependence in Fig. 9 is $\mathrm{Re}D(\omega) \propto \omega^s$, $s \sim 0.8$. Thus, if the approximation in (18) using an average Δ, is any good, the temperature dependence for $\mathrm{Re}D(\omega)$ should follow from (40); i.e., the data points in Fig. 9 (for $T <$ ionization region) should lie on four parallel lines, with slope corresponding to $(1 - s)\Delta$. The temperature dependence of $\mathrm{Re}D(\omega)$ in Fig. 9 is complicated by the fact that there seems to be two separate sets of lines. A low-temperature set with slope corresponding to $(0.18)(1.7$ meV$)$ or $\Delta = 1.7$ meV and the higher-temperature set with slope $\sim (0.2)(12.7$
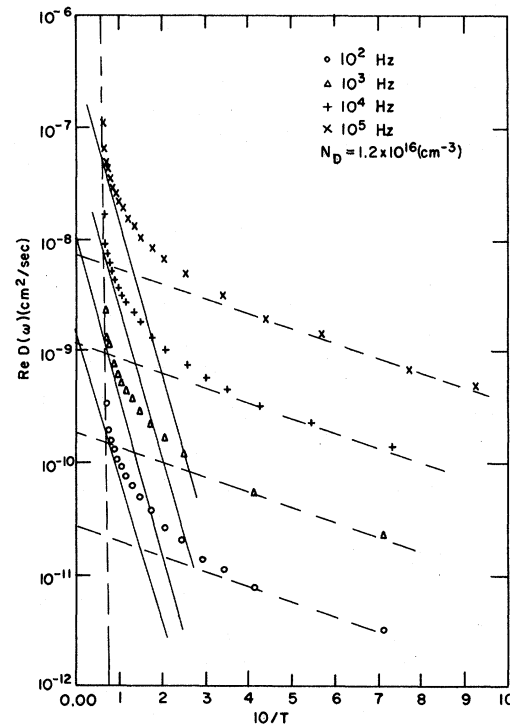
FIG. 9. Real part of the diffusion constant [derived from the measured values of $\mathrm{Re}\sigma(\omega)$ in Fig. 8 with the relation $\mathrm{Re}D(\omega)$ (cm^2/sec) $= (0.6723T)\mathrm{Re}\sigma(\omega)\,(\Omega^{-1}$ cm$^{-1})$] $\mathrm{Re}D(\omega)$ vs $10/T$. The solid and dashed lines are explained in the text (cf. Sec. III B).

meV) or $\Delta = 12.7$ meV. We will argue that the two values for Δ for the two temperature regions are evidence for two distinct hopping "channels." The low-temperature channel ($\Delta = 1.7$ meV) is associated with the more familiar hopping we have been discussing: An electron on a neutral donor in its ground state hops to the ground state of a vacant donor. The Δ is produced by the fluctuations in the ground-state energy of the donors, which in turn is due to the presence of ionized donors and acceptors. Although the dc impurity conductivity of the sample under consideration (in Fig. 9), $N_D = 1.2 \times 10^{16}$ cm^{-3}, $K = 0.066$, has not been measured [according to the theoretical results in Fig. 5 even at high temperature, $T \sim 20°$, the dc impurity conductivity would be very small, $\sigma(0) \sim 10^{-19}$ Ω^{-1}cm^{-1}], one can still obtain an estimate of $\Delta_{\rm expt}$. Using the sample parameters, in (50) Δ (ESY) $= 2.2$ meV, and for Δ (MA) we must use Table II in Ref. 3, since $K > 0.03$, to obtain Δ (MA) $= 2.13$ meV. Thus, $\Delta_{\rm expt} \sim 2.0$–$2.2$ meV and 1.7 meV$/\Delta_{\rm expt} \sim 0.8$. With this estimate, one sees that $\Delta = 1.7$ meV, obtained from the low-temperature slope in Fig. 9, is a very reasonable value for the effective activation energy in the ac hopping regime. Further, the fact that $\Delta/\Delta_{\rm expt} \sim 80\%$ is consistent with the discussion above, that the effective Δ for the low-concentration samples is almost frequency independent, i.e., $\Delta(r, \theta)$ [cf. (19)] has a slow spatial variation.

The high-temperature channel ($\Delta = 12.7$ meV), we claim, is hopping between an electron in the ground state on a neutral donor to the (excited) split ground state of a vacant donor. According to the effective-mass theory[9] the wave function of the ground state of the P impurity in Si is a linear combination of the "simple effective-mass" wave functions, each associated with one of the six conduction-band minima. Thus, the P-donor ($1s$, $m = 0$) ground state is sixfold degenerate. This degeneracy is partially lifted by the interaction of the completely symmetrical (A_1) state with the donor nucleus, thus producing corrections to the effective-mass ground state (valley-orbit splitting). The splitting of the $1s$, $m = 0$ state is the difference between the observed ground-state energy and the effective-mass value; for P donor[29] in Si it is 13 ± 3 meV. The lowest excited state[29] ($2p$, $m = 0$) is 34 meV above the ground state. Hence, $\Delta = 12.7$ meV, obtained by dividing the (apparent) activation energy, corresponding to the slope of the solid lines in Fig. 9, by $1 - s$, is in good agreement with the ground-state splitting 13 ± 3 meV. The proposed hopping mechanism is, thus, plausible. The first basic question is: Are the two hopping channels, with such a large difference in activation energy (a factor of 7.5), compatible? To answer this we *sketch* a theory for the two distinct hopping

channels. Returning to (9), we write

$$Q(t) = \exp\left(-\sum_j [W_1(\vec{r}_j) + W_2(\vec{r}_j)] t\right), \tag{52}$$

where $W_{1,2}(\vec{r}_i)$ is the transition rate with activation energy $\Delta_{1,2}$ and $\Delta_1 \ll \Delta_2$. Again, computing the configuration average, as in (10), one can obtain

$$\ln\langle Q(t)\rangle = -N_D \int d^3r\{1 - \exp[-W_1(\vec{r})t]\}$$
$$- N_D \int d^3r [1 - \exp(-W_2(\vec{r})t)]. \tag{53}$$

The main point to be emphasized in the structure of (53), is that, as a consequence of configuration averaging, for *parallel decay channels one does not add the transition rates to determine a net rate*, $W_{\rm net}(\vec{r}) = \sum_{i,j} W_i(\vec{r}_j)$, *but one adds weighted values of* $1 - \exp[-W_i(\vec{r}_j)t]$. Proceeding one step further, using (18) for $W(\vec{r})$ and (24), one has, explicitly,

$$\ln\langle Q(t)\rangle = -(\tfrac{4}{3}\pi N_D)r_{T(1)}^3 - (\tfrac{4}{3}\pi N_D)r_{T(2)}^3, \tag{54}$$

where

$$r_{T(i)} = R_d^{(i)} \ln(e^\gamma W_0^{(i)} e^{-\Delta_i/kT} t). \tag{55}$$

So, without a great deal of more detail, even though $r_{T(1)} \gg r_{T(2)}$ at low temperature, they can become comparable at higher temperatures (especially as $R_d^{(2)} > R_d^{(1)}$ and $W_0^{(2)} > W_0^{(1)}$). When the latter occurs, the temperature dependence of the second term on the right-hand side of (54) will obviously dominate the temperature dependence of $\langle Q(t)\rangle$. We will put the whole discussion on a more intuitive basis: At higher temperatures, to satisfy the condition in (24), $W_i(\vec{r})t \sim 1$, for fixed t, the Δ_1 channel includes larger interdonor hops, while the Δ_2 channel can provide hops with comparable transition rates using shorter interdonor distances.[31]

The second basic question is: What are other possible mechanisms? One could try to interpret the temperature dependence of Re$D(\omega)$ in Fig. 9 as the transition to a dc impurity conduction [with a $\Delta_{\rm expt} = 2.54$ meV, i. e., $(0.2)(12.7 \text{ meV}) = 2.54$ meV] similar to the behavior of Re$D(\omega)$ in Fig. 7. Besides the point that the theoretical value, from Fig. 5, is $\sigma(0)_{\rm max} \sim 10^{-19}$ Ω^{-1}cm^{-1}, the obvious feature of the transition in Fig. 7 is that the *frequency dependence diminishes* with increasing T. In Fig. 9 the frequency dependence is Re$D(\omega) \propto \omega^{0.8}$ with increasing T until ionization (into the conduction band). Similarly, one may argue that the apparent change in activation energy for ac conductivity in Fig. 9 is analogous to the three activation energies (ϵ_i, $i = 1, 2, 3$) observed in the dc impurity conduction in n-type Ge and p-type Ge first studied extensively by Fritzsche[6,7,11] and, more recently, by Davis and Compton.[12] In this notation, ϵ_1 is associated with ionization (into the band), ϵ_3 with impurity hopping conduction, and ϵ_2 with some in-
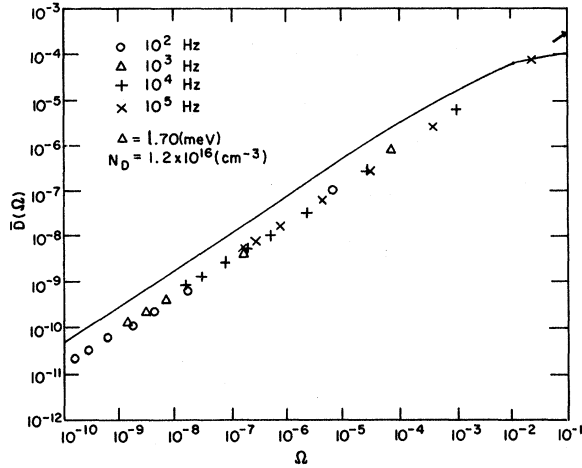
FIG. 10. Comparison of the theoretical (solid line) and experimental values of $\mathrm{Re}\bar{D}(\Omega)$. The dimensionless diffusion constant $\bar{D}(\Omega)/(\frac{1}{6}\sigma_{\mathrm{rms}}^2 e^\gamma W_M)$, with $\gamma = 0.5772$; Ω $\equiv \omega/W_M e^\gamma$, with $e^\gamma W_M = \bar{W}_0 \exp(-\Delta/\kappa T)$; $\bar{W}_0$ defined in Eq. (41). The experimental values of $\mathrm{Re}\bar{D}(\Omega)$ are derived from the values for $\mathrm{Re}D(\omega)$ in Fig. 9 for $10/T > 1.7$ (one data point, $10/T = 9.32$, $\omega/2\pi = 10^5$ Hz is off scale, as indicated by arrowhead above) with $\sigma_{\mathrm{rms}} = \bar{r} = 0.6r_D$ (cf. text at the end of Sec. III B), $\Delta = 1.7$ meV, $W_0' = 0.82 \times 10^{12}/$ meV sec [cf. Eq. (41)]. The theoretical curve for $\mathrm{Re}\bar{D}(\Omega)$ is reproduced from Fig. 5.

termediate conduction process. The various theories of ϵ_2 are reviewed in Ref. 12. Fritzsche[6] suggested ϵ_2 could be the energy required to put a second electron onto a neutral donor site (i.e., a transition to a D^- band). Thus, the higher-temperature conduction process in Fig. 9 could be the ϵ_2 one showing up in an ac measurement. We rule this possibility out because all the theories described for ϵ_2 involve a transition from a localized transport mode to a delocalized transport mode in some kind of intermediate band. Again, such a transition would necessitate the decrease in frequency dependence of $\mathrm{Re}D(\omega)$ with increasing T. The significance of the above discussion points out the importance of *both* simultaneous measurement of frequency and temperature dependence in the study of these conduction processes (e.g., in amorphous materials[32]).

We have not yet[31] worked out the theory with the two hopping channels present simultaneously, but have merely assumed the temperature dependence of each one to dominate in their respective regions. In Fig. 10, we plot the low-temperature data, $10/T > 1.7$ of Fig. 9, with $\Delta = 1.7$ meV and $\bar{W}_0 = 1.2 \times 10^{14}$ sec^{-1} and in Fig. 11 the higher-temperature data $10/T < 1.14$, with $\Delta = 12.7$ meV and $\bar{W}_0 = 2 \times 10^{15}$ [the $\bar{W}_0$ are determined from (41)]. The solid lines in Figs. 10 and 11 are the theoretical curves for $\mathrm{Re}D(\omega)$ reproduced from Fig. 5. In both Figs.

10 and 11, the agreement with theory for the frequency and temperature dependence is quite good. For hopping between the split ground states of the donors the assumption of a nearly constant Δ in (18) is expected to be a very reasonable one and with the choice of $\sigma_{\mathrm{rms}}^2 = 0.9 \; r_D^2$ (which is the average nearest-neighbor interdonor distance) the numerical agreement in Fig. 11 is excellent. It should be pointed out that the numerical agreement is quite insensitive to the value of $\bar{W}_0$ [cf. (40)]. In Fig. 10, the numerical agreement is off by an over-all factor of ~ 2.5, even though there has been a partial "fitting" to the theoretical calculation. The value of σ_{rms}^2 is chosen to conform to the values of the dominant intersite ac hopping distance used by PG in Table III of Ref. 5 for the same sample.[33] At 10 °K the lowest value of r in Table III of Ref. 5 is $r = 180$ Å. We have used $\sigma_{\mathrm{rms}} = 150$ Å at much lower temperatures. The smaller value for σ_{rms} is a partial compensation for the approximation of a constant Δ at these low temperatures. The variation of Δ in this low-concentration sample at low temperatures is still a factor in a careful numerical agreement[20] between theory and experiment.
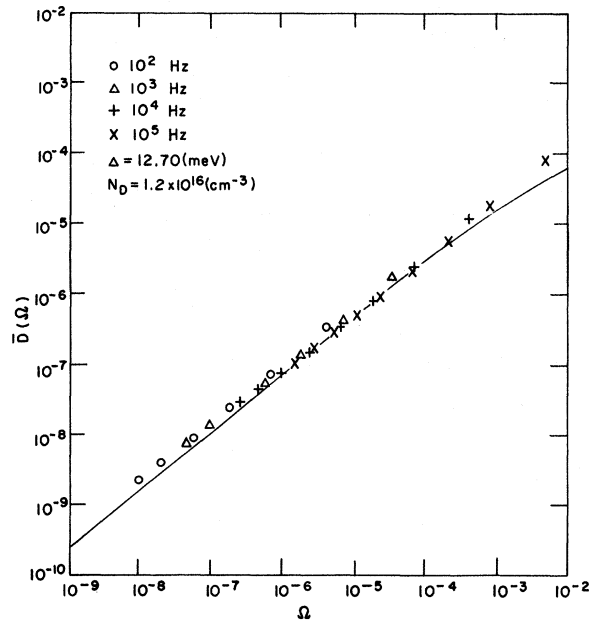
FIG. 11. Comparison of the theoretical (solid line) and experimental values of $\mathrm{Re}\bar{D}(\Omega)$. The dimensionless diffusion constant $\bar{D}(\Omega) = D(\omega)/(\frac{1}{6}\sigma_{\mathrm{rms}}^2 e^\gamma W_M)$, with $\gamma = 0.5772$; $\Omega \equiv \omega/W_M e$, with $e^\gamma W_M = \bar{W}_0 \exp(-\Delta/\kappa T)$; $\bar{W}_0$ defined in Eq. (41). The experimental values of $\mathrm{Re}\bar{D}(\Omega)$ are derived from the values for $\mathrm{Re}D(\omega)$ in Fig. 9 for $10/T < 1.14$, with $\sigma_{\mathrm{rms}} = \bar{r} = 0.9r_D$, $\Delta = 12.7$ meV, $W_0' = 0.82 \times 10^{12}/$meV sec [cf. Eq. (41)]. The theoretical curve for $\mathrm{Re}\bar{D}(\Omega)$ is reproduced from Fig. 5.

IV. CONCLUSION

In summary, the model stochastic process of a continuous-time random walk on a lattice has been demonstrated to be an excellent approximation for impurity hopping conduction in semiconductors. Even with the convenient simplification of assuming a constant energy fluctuation for the basic intersite transition rate, the theory is capable of correlating a considerable amount of experimental data (cf. Fig. 1). The general agreement with experiment lends credence to the main assumption of the model—the basic fluctuating quantity in hopping motion is the transition rate between the centers. The FT of the function $\psi(t)$ completely determines the frequency dependence of the conductivity and $\psi(t)$, in turn is simply related to the characteristic function of the sum of random transition rates (the parallel channels leaving a site). It is interesting that the CTRW with a single-site independent $\psi(t)$ seems to be an adequate approximation even though it is known that there are inequivalent hopping sites (depending on their proximity to the acceptor ion). One can generalize the CTRW to include two different $\psi(t)$. In fact the CTRW model of hopping transport can serve as a "theoretical laboratory," where one can examine the effects of more and more known details of hopping motion, e.g., using (19). Also, one can use the theory to parametrize the transport in amorphous materials[32] and polymeric systems[34] where the details of the microscopic process are not yet well understood.

ACKNOWLEDGMENTS

APPENDIX A: ANALYTIC EXPRESSION FOR $\psi(t)$

Inserting the expression for $W(\vec{r})$ in (14) (which depends only on $|\vec{r}|$) into (10), one has

$$\langle Q(t)\rangle = \exp\left[-4\pi N_D \int_0^\infty (1-e^{-W(r)t})r^2\,dr\right]$$

$$= \exp\left\{-\eta \int_0^\infty [1-\exp(-\tau e^{-x})]\,x^2\,dx\right\},$$
(A1)

with $\tau \equiv W_M t$ and $\eta \equiv 4\pi N_D R_d^3$. The x integral in the exponent of (A1) is integrated by parts and rewritten with a parameter a to obtain

$$\frac{\tau}{3}\int_0^\infty x^3 e^{-x}\exp(-\tau e^{-x})dx$$

$$= \frac{\tau}{3}\left[-\frac{d^3}{da^3}\int_0^\infty e^{-ax}\exp(-\tau e^{-x})dx\right]_{a=1}. \quad \text{(A2)}$$

Now,

$$\int_0^\infty e^{-ax}\exp(-\tau e^{-x})\,dx = \tau^{-a}\,\gamma(a,\tau)\,, \quad \text{(A3)}$$

where $\gamma(a,\tau)$ is the incomplete Γ function.[21] Thus, the exponent in (A1) is

$$\frac{-\eta\tau}{3}\left(\frac{-d^3}{da^3}\tau^{-a}\gamma(a,\tau)\right)_{a=1}. \quad \text{(A4)}$$

For large τ $(\tau > 10)$,

$$\gamma(a,\tau) \simeq \Gamma(a) - \tau^{a-1}e^{-\tau}$$

$$\times\left(1 + \frac{a-1}{\tau} + \frac{(a-1)(a-2)}{\tau^2} + \cdots\right).$$

Therefore,

$$-\frac{d^3}{da^3}\tau^{-a}\gamma(a,\tau)\bigg|_{a=1} \simeq -\frac{d^3}{da^3}\tau^{-a}\Gamma(a)\bigg|_{a=1}$$

$$+\frac{6e^{-\tau}}{\tau^4}\left(1-\frac{6}{\tau}+\cdots\right).$$

Dropping the second term on the right-hand side, the first term is equal to

$$\frac{1}{\tau}\left\{\left[\ln\tau - \left(\frac{d\ln\Gamma(a)}{da}\right)_{a=1}\right]^3 + 3\left[\ln\tau - \left(\frac{d\ln\Gamma(a)}{da}\right)_{a=1}\right]\right.$$

$$\left.\times\left(\frac{d^2\ln\Gamma(a)}{da^2}\right)_{a=1} - \left(\frac{d^3\ln\Gamma(a)}{da^3}\right)_{a=1}\right\}, \quad \text{(A5)}$$

the derivatives in (A5) are just the polygamma functions.[21] Thus,

$$\langle Q(t)\rangle = \exp\left\{-\tfrac{1}{3}\eta\left[(\ln e^\gamma\tau)^3 + 3\zeta(2)\ln e^\gamma\tau + 2\zeta(3)\right]\right\}, \quad \text{(A6)}$$

where $\gamma = 0.5772\ldots$, $\zeta(2) = 1.645\ldots$, $\zeta(3) = 1.202\ldots$. The series expansion of (A3) is

$$\tau^{-a}\gamma(a,\tau) = \sum_{n=0}^\infty \frac{(-\tau)^n}{(a+n)n!}\,; \quad \text{(A7)}$$

hence (A4) is equal to

$$-2\eta\tau\sum_{n=0}^\infty \frac{(-\tau)^n}{(1+n)^4 n!} \quad \text{(A8)}$$

and

$$\langle Q(t)\rangle = \exp\left(2\eta\sum_{n=1}^\infty \frac{(-\tau)^n}{n^4(n-1)!}\right). \quad \text{(A9)}$$

For small τ $(\tau < 1)$,

$$\langle Q(t)\rangle = 1 - 2\eta\tau + (\tfrac{1}{8}\eta + 2\eta^2)\tau^2 + \cdots. \quad \text{(A10)}$$

Thus,

$$\psi(t)/W_M = 2\eta - (\tfrac{1}{4}\eta + 4\eta^2)\tau + \cdots. \quad \text{(A11)}$$

APPENDIX B: EVALUATION OF $\bar{Q}(\Omega)$ BY SADDLE-POINT METHOD

The Fourier transform (FT) of $\psi(t)$ determines the ac diffusion constant $D(\omega)$. In the following, we use the saddle-point integration technique as a general method to obtain $\tilde{\psi}(i\omega)$. A purely numerical evaluation, using the fast Fourier transform is not adequate, as the range of interest for ω spans many decades.

We first rewrite $\tilde{\psi}(i\omega)$, using (18), as

$$\tilde{\psi}(i\omega) = 1 - i\Omega\bar{Q}(\Omega) , \tag{B1}$$

where $\Omega = \omega e^{-\gamma}/W_M$ and

$$\bar{Q}(\Omega) = \int_0^\infty d\tau \, e^{-i\Omega\tau}Q(\tau) . \tag{B2}$$

We shall be interested throughout in the FT of $Q(\tau)$ in (B2) for $\Omega \ll 1$. In that case, with

$$\bar{Q}(\Omega) = \int_0^1 d\tau \, e^{-i\Omega\tau}Q(\tau) + \int_1^\infty d\tau \, e^{-i\Omega\tau}Q(\tau) , \tag{B3}$$

the first integral being of order unity [cf. (A10)], and the second of order Ω^{-1} (the effective range of τ), one has

$$\bar{Q}(\Omega) \simeq \int_1^\infty d\tau \, e^{-i\Omega\tau}Q(\tau) . \tag{B4}$$

The large τ form of $Q(\tau)$ can now be used in (B4) [cf. (A6)] and with a change of variable, $x = \ln\tau$,

$$\bar{Q}(\Omega) = \int_0^\infty dx \exp[x - i\Omega e^x - (\tfrac{1}{3}\eta)x^3] . \tag{B5}$$

To use the saddle-point method[24] the integral in (B5) is recast as a contour integral in the complex z plane ($z = x + iy$),

$$\bar{Q}(\Omega) = \int_I dz \, e^{\Phi(z)} , \tag{B6}$$

with I = real line ($x > 0$) and

$$\Phi(z) \equiv z - i\Omega e^z - (\tfrac{1}{3}\eta)z^3 ; \tag{B7}$$

$\Phi(z)$ is analytic in the finite z plane. The contour of integration is now distorted to pass through a saddle point of $e^{\Phi(z)}$ along a path of steepest descent: $\text{Im}\Phi(z) = \text{Im}\Phi(z_0)$, where z_0 is a stationary point of $\Phi(z)$, i.e., $\Phi'(z_0) = 0$.

1. Stationary Points of $\Phi(z)$

To obtain the stationary points of $\Phi(z)$ we set the derivative

$$\Phi'(z) = 1 - i\Omega e^z - \eta z^2 \tag{B8}$$

equal to zero, i.e.,

$$\text{Re:} \quad 1 - \eta(x_0^2 - y_0^2) + \Omega e^{x_0}\sin y_0 = 0 , \tag{B9}$$

$$\text{Im:} \quad 2\eta x_0 y_0 + \Omega e^{x_0}\cos y_0 = 0 . \tag{B10}$$

To solve (B9) and (B10) for x_0, y_0, we first substitute

$$\Omega e^{x_0} = -2\eta x_0 y_0/\cos y_0 \tag{B11}$$

from (B10) into (B9),

$$x_0^2 + 2x_0 y_0 \tan y_0 - \eta^{-1} - y_0^2 = 0 . \tag{B12}$$

Now, (B12) is solved for x_0 in terms of y_0,

$$x_0 = [(y_0 \tan y_0)^2 + y_0^2 + \eta^{-1}]^{1/2} - y_0 \tan y_0 , \tag{B13}$$

where the plus sign of the radical is chosen so that $x_0 \geq 0$ (which corresponds to $\tau > 1$). The right-hand side of (B13) will be designated $x_0(y_0)$ and note it is an even function of y_0. In the present calculation we consider a range of N_D such that $\eta^{-1} > 166.66$; thus for $|y_0| < \tfrac{1}{2}\pi$, $x_0(y_0) \simeq \eta^{-1/2}$. As $y_0 \to (\tfrac{1}{2}\pi)_-$, $\tan y_0 \to +\infty$, and $x_0(y_0) \to 0$, but as $y_0 \to (\tfrac{1}{2}\pi)_+$, $\tan y_0 \to -\infty$, and $x_0(y_0) \to +\infty$. In the intervals $(n + \tfrac{1}{2})\pi < y_0 < (n + \tfrac{3}{2})\pi$ ($n = 0, 1, 2, \ldots$), $x_0(y_0)$ monotonically decreases from $+\infty \to 0$. We insert $x_0(y_0)$ into (B10) and determine y_0 from the graphic solution of

$$-e^{x_0(y_0)}\cos y_0/x_0(y_0)y_0 = 2\eta/\Omega . \tag{B14}$$

The left-hand side of (B14) is an odd function of y_0 and also it is an explicit function of η. In Fig. 12 we plot the positive values of the left-hand side of (B14) for $\eta = 6\times10^{-3}$ (i.e., $N_D = 2.7\times10^{17}$ cm^{-3}). The solutions $y_0(\Omega, \eta)$ of (B14) are simply obtained by the intercepts of this plot with the horizontal
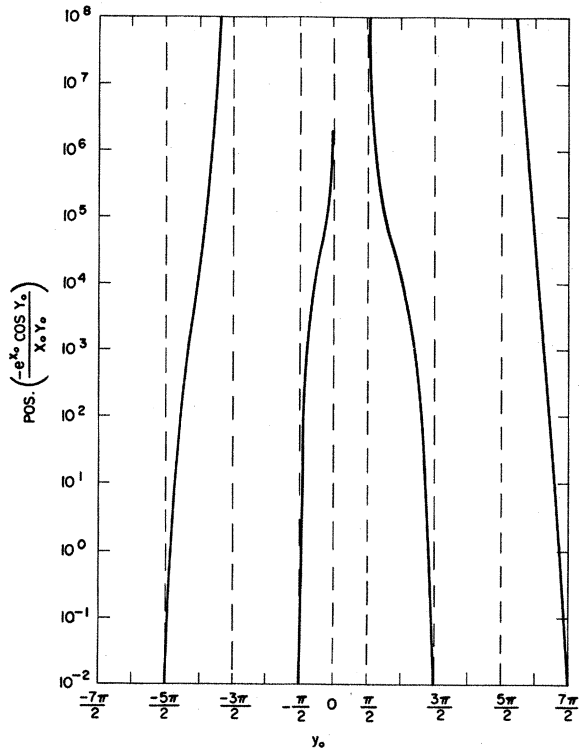
FIG. 12. Positive values of the function $f(y_0) = e^{-x_0}\cos y_0/x_0 y_0$ vs y_0, used in the graphic solution for the stationary point z_0 of $\Phi(z)$ [cf. Eq. (B7)]. $f(y_0)$ is evaluated using Eq. (B13) for x_0 and $\eta = 6\times10^{-3}$. Solutions for $y_0(\Omega)$ are intercepts of $f(y_0)$ with the horizontal lines corresponding to the different values of $2\eta/\Omega$.
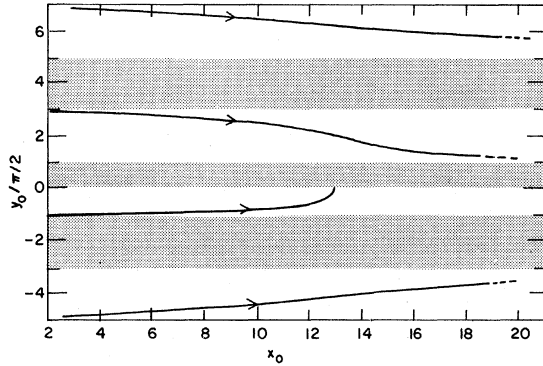
FIG. 13. Trajectories of the stationary points $z_0(\Omega)$ $=x_0(\Omega)+iy_0(\Omega)$ of $\Phi(z)$ [cf. Eq. (B7)] as a function of decreasing Ω (indicated by arrow). The trajectories lie in nonoverlapping strips.

lines associated with each value of $2\eta/\Omega$. The corresponding values of x_0 are obtained with $y_0(\Omega, \eta)$ inserted into (B13).

As evident from the plot there are multiple solutions of $\Phi'(z_0)=0$. In Fig. 13 the trajectories of $z_0(\Omega)$ are shown, with the arrow indicating the direction of decreasing Ω. Each group of $z_0(\Omega)$ lie in nonoverlapping strips parallel to the real axis with the strip $(-\frac{1}{2}\pi < y_0 \leq 0)$, adjoining the real axis, containing the solution with the correct limiting dc value (cf. below). The other solutions give exponentially decreasing contributions as $\Omega \to 0$. Therefore the contour in (B6) is distorted to pass through the saddle point just below the real axis and lie along a path of steepest descent. There is no "interference" along this path from any other saddle points.

2. Leading Asymptotic Term for $\tilde{Q}(\Omega)$

The leading term in the asymptotic expansion of $\tilde{Q}(\Omega)$ is

$$\tilde{Q}(\Omega) \simeq e^{\Phi(z_0)}[-\Phi''(z_0)/2\pi]^{-1/2} , \qquad (B15)$$

where

$$\Phi(z_0) = z_0 - (\tfrac{1}{3}\eta)z_0^3 - 1 + \eta z_0^2 , \qquad (B16)$$

$$-\Phi''(z_0) = 1 + 2\eta z_0 - \eta z_0^2 , \qquad (B17)$$

using the relation $i\Omega e^{z_0} = 1 - \eta z_0^2$. The leading term is obtained by simply considering the contribution to the integral (B6) in the neighborhood of the saddle point. The phase in (B15) is determined in a manner to insure that the integration contour passes through the saddle point along a path of steepest descent.[24] The full asymptotic expansion can be obtained by taking account of the entire path of steepest descent.[24] In Fig. 3 we plot $x_0(\Omega)$ and $y_0(\Omega)$ for $\eta = 6 \times 10^{-3}$, also for comparison the straight line, $-\ln\Omega$. Calculating z_0 for other val-

ues of η, we conclude

$$-\ln\Omega < \eta^{-1/2} \begin{cases} x_0 \simeq -\ln\Omega - \eta(\ln\Omega)^2 \\ -y_0/(\tfrac{1}{2}\pi) \simeq 1 - 2\eta(-\ln\Omega) \end{cases} . \qquad (B18)$$

These results are obtained by inserting $x_0 = -\ln\Omega + \epsilon$ and $-y_0 = \tfrac{1}{2}\pi(1-\delta)$ into (B9) and (B10) and retaining linear terms in ϵ, δ. Such a procedure was suggested by the *numerical* results obtained in Fig. 3, for the region

$$-\ln\Omega > \eta^{-1/2} \begin{cases} x_0 \simeq \eta^{-1/2} \\ y_0 = -\tfrac{1}{2}\Omega\eta^{-1/2}e^{\eta^{1/2}} \end{cases} . \qquad (B19)$$

[The last result follows from substituting $x_0(y_0) = \eta^{-1/2}$ into (B14) and assuming $y_0 \ll 1$.]

Inserting (B18) into (B15),

$$-\ln\Omega < \eta^{-1/2} ,$$

$$\tilde{Q}(\Omega) \simeq (ie\Omega)^{-1}$$

$$\times \exp\{-\eta[\tfrac{1}{3}(-\ln\Omega - \tfrac{1}{2}i\pi)^3 + \cdots]\}(2\pi)^{1/2}$$

or, roughly, $\tilde{Q}(\Omega) \propto \Omega^{-[1-\delta(\Omega)]}$, where $\delta(\Omega)$ varies slowly with Ω. In the dc limit $\Omega \to 0$, [cf. (B19)] $x_0 \to \eta^{-1/2}$, $y_0 \to 0_-$,

$$\Phi(z_0) \to \tfrac{2}{3}\eta^{-1/2} , \quad -\Phi''(z_0) \to 2\eta^{1/2} ; \qquad (B20)$$

hence,

$$\tilde{Q}(0) \simeq e^{2\eta^{-1/2}/3}(\eta^{1/2}/\pi)^{-1/2} . \qquad (B21)$$

The value for $\tilde{Q}(0)$ in (B21) is in agreement with the asymptotic evaluation[21] of the exact result

$$\tilde{Q}(0) = \eta^{-1/3}\pi \text{Hi}(\eta^{-1/3}) \qquad (B22)$$

in (42) in the text.

The characteristic frequency in this model, using the simple transition rate, for marking the change from ac to essentially dc behavior is $\Omega_c = e^{-\eta^{-1/2}}$. A simple interpretation of this value for Ω_c follows from an examination of (B5). The peak of the function $\exp[x - (\tfrac{1}{3}\eta)x^3]$ occurs at the maximum of the exponent: $x_c = \eta^{-1/2}$. For Ω such that $\Omega e^x \simeq 1$, for $x < x_c$ (i.e., $-\ln\Omega < \eta^{-1/2}$), the $\exp(-i\Omega e^x)$ term acts as an effective "cutoff." However, for $-\ln\Omega > \eta^{-1/2}$, the factor $\exp(-i\Omega e^x)$ no longer acts as a "cutoff" because the function $\exp[x - (\tfrac{1}{3}\eta)x^3]$ is dropping rapidly for $x > x_c$, i.e., it is already "cutoff," hence, $\exp(-i\Omega e^x)$ is superfluous in effectively modulating the area under curve. Therefore, for $\Omega < \Omega_c$ there is essentially no Ω dependence of the integral in (B5).

The complete numerical results for

$$e^{-\eta}D(\omega)/\tfrac{1}{6}\sigma_{rms}^2 W_M \equiv \bar{D}(\Omega) = \tilde{Q}(\Omega)^{-1} - i\Omega , \qquad (B23)$$

for $N_D = 2.7 \times 10^{17}$ cm^{-3} and $N_D = 10^{16}$ cm^{-3} are shown in Figs. 4 and 5 and discussed in the accompanying text.

3. Higher-Order Asymptotic Terms for $\tilde{Q}(\Omega)$

The expansion parameter for the asymptotic series for $\tilde{Q}(\Omega)$ is not obvious for the region:

$-\ln\Omega < \eta^{-1/2}$. For the region $-\ln\Omega > \eta^{-1/2}$, one can assume $\Omega \to 0$ and use the asymptotic series for the Airy functions[21]

$$\bar{Q}(0) = \eta^{-1/3}\,\pi\,\text{Hi}(\eta^{-1/3})$$

$$\sim \pi^{1/2}\eta^{-1/4}e^{2\eta^{-1/2}/3}\sum_{k=0}^{\infty}C_k\left(\frac{3\eta^{1/2}}{2}\right)^k, \quad (B24)$$

where

$$C_k = \Gamma(3k+\tfrac{1}{2})/[54^k k!\,\Gamma(k+\tfrac{1}{2})]\;; \quad (B25)$$

clearly the asymptotic expansion parameter is $\eta^{-1/2}$.

For the general case we follow the procedure in Morse and Feshbach[35] and derive for the first two terms:

$$\bar{Q}(\Omega) \sim e^{\Phi^{(z_0)}}[2/-\Phi''(z_0)]^{1/2}(1+C), \quad (B26)$$

$$C \equiv \tfrac{1}{2}\left[\tfrac{5}{12}(1+2\eta-\eta z_0^2)^2(1+2\eta z_0-\eta z_0^2)^{-3}\right.$$
$$\left. -\tfrac{1}{4}(1-\eta z_0^2)(1+2\eta z_0-\eta z_0^2)^{-2}\right]. \quad (B27)$$

The dependence of C in (B27) on Ω, η is rather complicated, however, we make the following simple observations: For $-\ln\Omega < \eta^{-1/2}$, C is nearly constant and at most $C \simeq 0.1$. For $-\ln\Omega > \eta^{-1/2}$, $z_0 \to \eta^{-1/2}$ and $C \to \tfrac{5}{48}\eta^{1/2}$, which is identical to the second term of the sum in (B24). Thus, C is at most $\sim 10\%$ correction for the range of Ω, η considered here.

[1]H. Scher and M. Lax, preceding paper, Phys. Rev. B 7, 4491 (1973).

[2]E. W. Montroll and G. H. Weiss, J. Math. Phys. 6, 167 (1965).

[3]A. Miller and E. Abrahams, Phys. Rev. 120, 745 (1960).

[4]N. F. Mott and W. D. Twose, Advan. Phys. 10, 107 (1961).

[5]M. Pollak and T. H. Geballe, Phys. Rev. 122, 1742 (1961).

[6]H. Fritzsche, J. Phys. Chem. Solids 6, 69 (1958).

[7]H. Fritzsche and M. Cuevas, Phys. Rev. 119, 1230 (1960).

[8]W. Kohn and J. M. Luttinger, Phys. Rev. 98, 915 (1955).

[9]W. Kohn, in Solid-State Physics, edited by F. Seitz and D. Turnbull (Academic, New York, 1957), Vol. 5, p. 257.

[10]J. Blinowski and J. Mycielski, Phys. Rev. 136, A266 (1964); Phys. Rev. 140, A1024 (1965).

[11]C. S. Hung and J. R. Gliessman, Phys. Rev. 79, 726 (1950); G. Busch and H. Labhart, Helv. Phys. Acta. 19, 463 (1946); H. Fritzsche, Phys. Rev. 99, 406 (1955); S. H. Koenig and R. Gunther-Mohr, J. Phys. Chem. Sol. 2, 268 (1957); H. Fritzsche and K. Lark-Horovitz, Phys. Rev. 113, 999 (1959); H. Fritzsche, Phys. Rev. 119, 1899 (1960); P. Csavinsky, Phys. Rev. 119, 1605 (1960); K. R. Atkins, R. Donovan, and R. H. Wahnsley, Phys. Rev. 118, 411 (1960); R. Keyes and R. J. Sladek, J. Phys. Chem. Solids 2, 143 (1956); R. J. Sladek and R. W. Keyes, Phys. Rev. 122, 437 (1961); R. K. Ray and H. Y. Fan, Phys. Rev. 121, 768 (1961); S. Golin, Phys. Rev. 132, 178 (1963); M. Pollak and D. H. Watt, Phys. Rev. 140, A87 (1965).

[12]E. A. Davis and W. Dale Compton, Phys. Rev. 140, A2183 (1965).

[13]N. F. Mott, Can. J. Phys. 34, 1356 (1956); E. M. Conwell, Phys. Rev. 103, 51 (1956); P. J. Price, Phys. Rev. 104, 1223 (1956); T. Kasuya and S. Koide, J. Phys. Soc. Japan 13, 1287 (1958); R. Jones and W. Schiach, J. Phys. C: Solid State Phys. 5, 43 (1972); W. Brenig, G. Döhler, and P. Wölfle, Z. Physik 246, 1 (1971).

[14]V. Ambegaokar, B. I. Halperin, and J. S. Langer, Phys. Rev. B 4, 2612 (1971); M. Pollak, J. Non-Crystalline Solids 11, 1 (1972).

[15]M. Pollak, Phys. Rev. 133, A564 (1964).

[16]M. Pollak, Phys. Rev. 138, A1822 (1965).

[17]D. G. Thomas, J. J. Hopfield, and W. M. Augusty-niak, Phys. Rev. 140, A202 (1965); D. G. Thomas, J. J. Hopfield, and K. Colbow, in Seventh International Conference on the Physics of Semiconductors (Dunod, Paris, 1964), Vol. 4, p. 67.

[18]R. C. Enck and A. Honig, Phys. Rev. 177, 1182 (1969).

[19]M. Lax, Rev. Mod. Phys. 38, 541 (1966), Eq. (2.30).

[20]H. Scher and M. Lax (unpublished).

[21]Handbook of Mathematical Functions, edited by M. Abramowitz and I. A. Stegun (National Bureau of Standards, Washington, D. C., 1964).

[22]D. Bedeaux, K. Lakatos-Lindenberg, and K. E. Schuler, J. Math. Phys. 12, 2116 (1971).

[23]M. Pollak (private communication).

[24]E. T. Copson, Asymptotic Expansions (Cambridge U.P., Cambridge, England, 1965).

[25]Thus the set of curves in Fig. 5 are Kramers-Kronig (KK) transform pairs of each other; likewise for the set in Fig. 4. Exhibiting the KK pairs for $\sigma(\omega)$ over the entire width of the experimental frequency range $(0-10^5$ Hz) obviates the need for the artificial separation of $\sigma(\omega)$ into a σ_{dc} and σ_{ac}.

[26]M. Pollak has been kind enough to send us the original data used in Fig. 5 (PG). In addition, unpublished measurements of the dc impurity conduction for sample No. 12 $(N_D = 1.1 \times 10^{17}$ cm$^{-3})$ are included in this data set, which we refer to in the text and in Table II.

[27]In Ref. 19 of Paper I, we show $\sigma_{\text{rms}}^2(\omega) \to 0.9 r_D^2$ for $\omega \to 0$, using (1), (16) and (18).

[28]A. L. Efros, B. I. Shklovskii, and I. Y. Yanchev, Phys. Stat. Sol. (B) 50, 45 (1972).

[29]Reference 9, p. 293.

[30]R. A. Smith, Semiconductors (Cambridge U.P., Cambridge, England, 1954), p. 90.

[31]The more complete theory of the distinct hopping channels [e.g., the calculation of $Q(\Omega)$] is formally a special case of including the θ dependence in $\Delta(r, \theta)$. This theory is carried out in Ref. 20.

[32]A. I. Lakatos and M. Abkowitz, Phys. Rev. B 3, 1791 (1971).

[33]A clear need exists in this case to consider $\sigma_{\text{rms}}^2(\omega)$, as will be carried out in Ref. 19 of Paper I.

[34]M. A. Abkowitz, G. R. Pfister, and R. G. Crystal (unpublished).

[35]P. M. Morse and H. Feshbach, Methods of Theoretical Physics (McGraw-Hill, New York, 1953), pp. 441-442.